GAP FILLING OF HIGH-RESOLUTION SOIL MOISTURE FOR SMAP/SENTINEL-1: A TWO-LAYER MACHINE LEARNING-BASED FRAMEWORK WITH SPATIAL/TEMPORAL TRANSFER LEARNING

Hanzi Mao
Department of Computer Science and Engineering
Texas A&M University
College Station, TX 77843
hzmao@tamu.edu

Dhruva Kathuria
Biological and Agricultural Engineering
Texas A&M University
College Station, TX 77843
kathuria.dhruva@tamu.edu

Nick Duffield
Department of Electrical and Computer Engineering
Texas A&M University
College Station, TX 77843
duffieldng@tamu.edu

Binayak P. Mohanty
Biological and Agricultural Engineering
Texas A&M University
College Station, TX 77843
bmohanty@tamu.edu

ABSTRACT

As the most recent 3 km soil moisture product from the Soil Moisture Active Passive (SMAP) mission, the SMAP/Sentinel-1 L2_SM_SP product has a unique capability to provide global-scale 3 km soil moisture estimates through the fusion of radar and radiometer microwave observations. The spatial and temporal availability of this high-resolution soil moisture product depends on concurrent radar and radiometer observations which is significantly restricted by the narrow swath and low revisit schedule of the Sentinel-1 radars. To address this issue, this paper presents a novel two-layer machine learning-based framework where the brightness temperature and subsequently the soil moisture are predicted at gap areas. Combined with the transfer learning strategy, the proposed method is able to gap-fill soil moisture with higher accuracy at areas where the radiometer observations are available while the radar observations are missing. The effectiveness of the two-layer framework is validated against hold-out SMAP/Sentinel-1 3 km soil moisture estimates at three study areas with distinct climate regimes, Arizona, South Dakota, and Arkansas. Results indicate that our proposed method is able to reconstruct 3 km soil moisture at gap areas with higher Pearson correlation coefficient (mean R = 0.723/0.82/0.798, at Arizona/South Dakota/Arkansas) and lower unbiased Root Mean Square Error (mean ubRMSE = 0.029/0.029/0.08) when compared to 1) the SMAP 9 km soil moisture product (mean R = 0.471/0.765/0.523, mean ubRMSE = 0.036/0.032/0.109) and 2) the conventional one-layer machine learning model that directly downscales soil moisture from 9 km to 3 km (mean R = 0.532/0.76/0.69, mean ubRMSE = 0.036/0.033/0.092).

Keywords Soil Moisture · Machine Learning · Multi-Resolution Gap Filling · SMAP satellite · Sentinel-1 satellite · Spatial/Temporal Transfer Learning

1 Introduction

Soil moisture is an essential variable controlling the exchange of water and energy fluxes between the land surface and the atmosphere. Retrieving high-resolution soil moisture at local, regional and global scales is critical for best

agricultural and irrigation practices [1], weather and climate predictions [2, 3], biogeochemical process characterizations [4] and drought and flood predictions [5, 6]. To complement the sparsely distributed ground-sampled soil moisture measurements [7, 8, 9], various microwave remote sensing techniques have been developed over the last few decades to retrieve soil moisture estimates at global scale such as the Advanced Scatterometer [10], the Advanced Microwave Scanning Radiometer-EOS [11], the Soil Moisture and Ocean Salinity (SMOS) [12], the Soil Moisture Active Passive (SMAP) mission [13], and the Sentinel-1 mission [14]. These global microwave sensing soil moisture products have the advantage of capturing soil moisture heterogeneity over large spatial extents. This further benefits regional and global scale applications that are impacted by land-atmosphere interactions and/or soil moisture variability [15, 16, 17].

Existing microwave remote sensing techniques measure the near surface soil moisture (≤ 5 cm) indirectly through its relationship with water content and soil dielectric constant. They can be classified into two categories according to the source of their signals, 1) the active radar that measures the backscattered signal after transmitting an active pulse and 2) the passive radiometer that measures the land surface emissions. Radar observations are provided with high resolution that in turn can capture fine-scale ($\sim$1-3 km) soil moisture/land surface heterogeneity. In addition to soil moisture, they are also highly sensitive to surface roughness and vegetation, which reduces the accuracy of the produced soil moisture estimates [18, 19]. On the contrary, the relatively mature passive radiometer remote sensing has the ability to provide more accurate estimates of soil moisture due to the high sensitivity of its observations to soil moisture [20]. The high accuracy of the soil moisture estimates produced by the passive remote sensing is, however, compromised by its coarse resolution, $\sim$40 km for both the SMOS and SMAP passive soil moisture products [12, 21] and 9 km for the SMAP enhanced passive soil moisture product [22], which restricts the applications of the resulting soil moisture products to many regional hydro-climatological studies [23, 13, 24, 25].

Among the various methods that are proposed to downscale the coarse-scale soil moisture [26, 27], the fusion of radar and radiometer microwave observations is one of the most promising and robust techniques to provide high resolution (1-10 km) soil moisture estimates at global scale. The SMAP mission, specifically, adopts the active-passive retrieval algorithm proposed by [28]. In this two-layer retrieval algorithm, the radar backscatter measurements are first used to downscale the coarse-scale passive brightness temperature measurements, from which the high resolution soil moisture is then retrieved through the single channel algorithm (SCA) [29]. The original SMAP observatory was launched on January 31, 2015. Equipped with an L-band radiometer and an L-band radar as a single observation system, its mission was to combine 36 km resolution brightness temperature and 3 km resolution radar backscatter to provide 9 km resolution accurate soil moisture at global scale [13, 30].

Unfortunately, the SMAP L-band radar unexpectedly ceased its operation on July 7, 2015. To recover the capability of providing high resolution soil moisture, one possible solution was to replace the SMAP L-band radar measurements with the C-band radar measurements from the European Space Agency (ESA)'s Sentinel-1 radars, Sentinel-1A and Sentinel-1B [31, 32]. Many studies have investigated the performance of integrating the C-band active and the L-band passive observations to retrieve high resolution soil moisture, with promising results [31, 33, 34, 35].

As the most recent 3 km soil moisture product from the SMAP mission, the SMAP/Sentinel-1 L2_SM_SP product [36] adopts the SMAP active-passive retrieval algorithm to combine the 9 km brightness temperature measurements from the SMAP enhanced passive soil moisture product with the 3 km aggregated co-polarization (co-pol) and cross-polarization (cross-pol) backscatter measurements retrieved by the Sentinel-1 radars. One restriction of this product, however, is that the Sentinel-1 radar observations have much narrower swath width ($\sim$250 km) compared with the relatively wide swath width (1000 km) of the SMAP radar and radiometer. As the SMAP active-passive retrieval algorithm requires concurrent radar and radiometer observations, the narrow swath of the Sentinel-1 radar observations significantly reduces the spatial coverage of the resulting daily soil moisture product compared with the SMAP enhanced passive 9 km soil moisture product (Figure 1). The temporal resolution also drops from a 3-day revisit schedule to a 6-day one when using the collocated Sentinel-1A and Sentinel-1B radar backscatter observations [13, 31, 37]. Additionally, considering that the Sentinel-1A and Sentinel-1B sensors provide backscatter measurements with different swath patterns and interleaved revisit schedules, the temporal resolution further drops to 12 days or more for some locations. Thus, the narrow swath and low revisit schedule of the produced SMAP/Sentinel-1 3 km soil moisture product cannot achieve the required temporal resolution for many soil moisture related applications [27, 38].

This paper thus focuses on downscaling/gap-filling soil moisture at areas where the SMAP active-passive retrieval algorithm cannot be applied due to missing radar backscatter measurements. [26] and [27] outline the various techniques to downscale passive remote sensing soil moisture. The techniques that do not rely on concurrent radar observations can be applied to the gap-filling task of the SMAP/Sentinel-1 3 km soil moisture product, such as fusion of optical/thermal and microwave methods [39, 40, 41], data assimilation methods [42, 43], and machine learning methods [44, 45, 46, 47, 48]. Among these approaches, machine learning techniques have shown great potential to downscale soil moisture with its ability to handle noisy data and learning complex non-linear systems [49, 50]. Existing machine learning methods capture the relationship between coarse-scale and fine-scale soil moisture directly with the
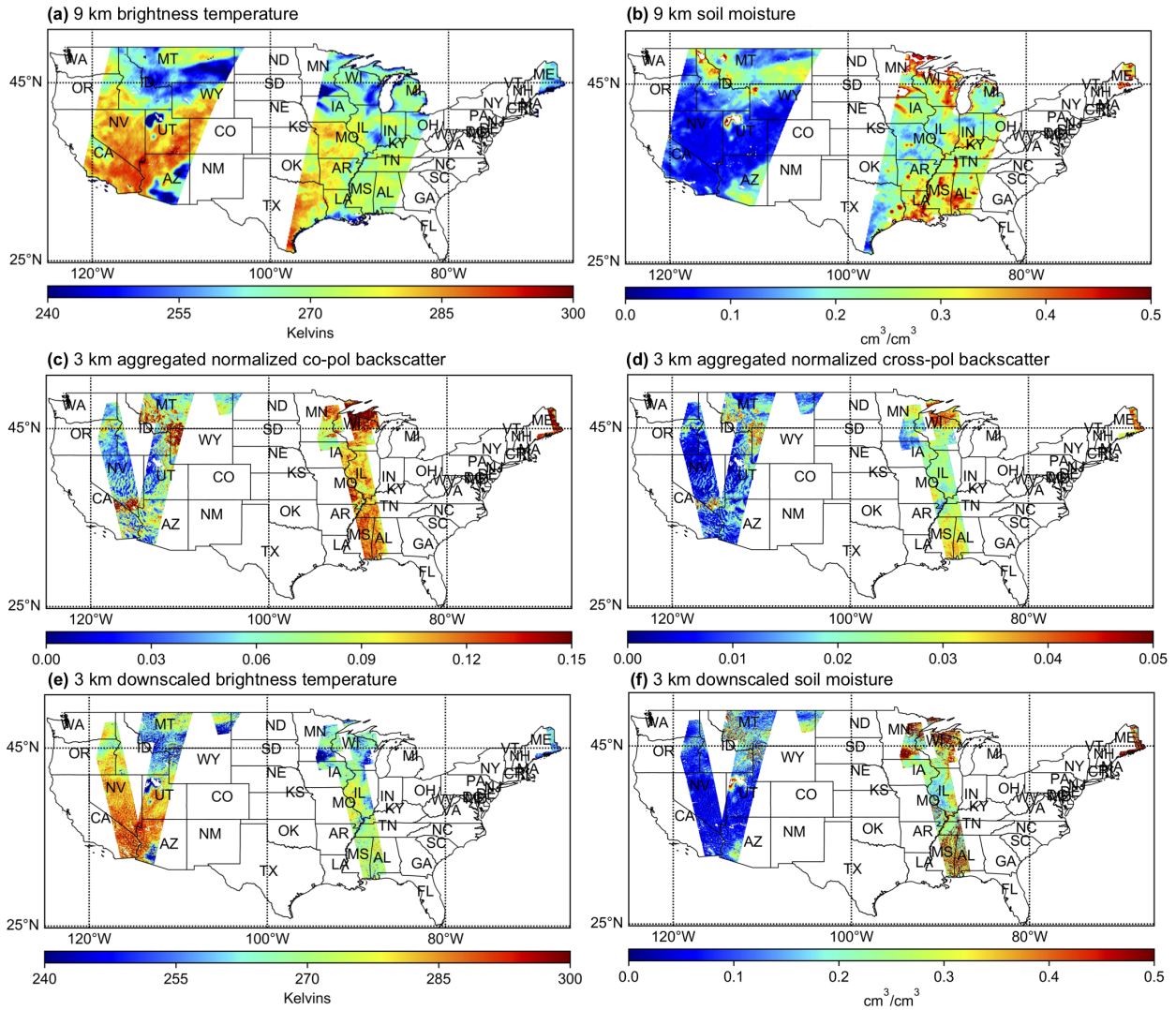
Figure 1: Spatial availability of the SMAP/Sentinel-1 active-passive 3 km soil moisture product (L2_SM_SP) and the SMAP enhanced passive 9 km soil moisture product (L3_SM_P_E) on June 16, 2018 for the Continental United States. (a) 9 km brightness temperature retrieved by the SMAP radiometer. (b) 9 km soil moisture converted from (a) using the single channel algorithm. (c) 3 km aggregated normalized co-pol backscatter retrieved by the Sentinel-1A/Sentinel-1B radars. (d) 3 km aggregated normalized cross-pol backscatter retrieved by the Sentinel-1A/Sentinel-1B radars. (e) 3 km downscaled brightness temperature from the SMAP active-passive retrieval algorithm. (f) 3 km downscaled soil moisture converted from (e) using the single channel algorithm.

aid of auxiliary environmental variables, such as soil properties, topography, land cover, and meteorological forcings. The fine-scale soil moisture estimates they use to train/calibrate the machine learning models are restricted to ground observed data that is from either catchment-scale campaigns [45, 48] or sparsely distributed soil moisture monitoring network [44].

In this paper, estimates from the SMAP/Sentinel-1 active-passive 3 km soil moisture product serve as target variables to train the machine learning models for the downscaling/gap-filling task. This greatly expands the training data size and has the potential to learn more complex relationship that exists between coarse-scale and fine-scale soil moisture [51]. Directly using remote sensing soil moisture estimates for training a machine learning model also has the advantage of maintaining high consistency, or "high fidelity" [52] between the downscaled predictions and the SMAP/Sentinel-1 3 km soil moisture product.

To exploit the 3 km estimates that are available at regional extent from the SMAP/Sentinel-1 product, we bring in a new learning strategy to the soil moisture gap-filling task, the transfer learning [53], that has been successful in many practical machine-learning applications [54, 55, 56]. Transfer learning, also known as the knowledge transfer, can be applied to applications where the training and test data have different input feature (or covariate) spaces and distributions. The hypothesis of transfer learning is that knowledge learned in one task (the training data) can be transferred to another task (the test data) with satisfactory predictive performance. This fits well for the soil moisture downscaling/gap-filling problem which is the primary focus of this paper. Relationship between the SMAP/Sentinel-1 3 km soil moisture/brightness temperature and the input features (including the SMAP enhanced 9 km soil moisture/brightness temperature and additional ancillary information such as soil properties, topography, etc.) can be learned through machine learning models at areas where both the Sentinel radar and SMAP radiometer observations, thus the 3 km soil moisture/brightness temperature, are available. The learned models can then be applied to predict 3 km soil moisture/brightness temperature at spatially/temporally neighboring gap areas where the Sentinel radar observations, and thus the downscaled soil moisture and brightness temperature, are missing.

Additionally, we propose in this paper a two-layer machine learning-based framework motivated by the SMAP active-passive retrieval algorithm to further improve the consistency between the downscaled soil moisture and the retrieved 3 km soil moisture from the SMAP/Sentinel-1 soil moisture product. The downscaled brightness temperature and soil moisture are predicted consecutively in two layered machine learning models. Instead of directly downscaling the 9 km soil moisture from the SMAP enhanced passive soil moisture product to 3 km, the 9 km brightness temperature (from the same product) is first downscaled to 3 km through a machine learning model. A separate machine learning model is then applied to convert the 3 km downscaled brightness temperature to 3 km soil moisture. This machine learning approach, different from the SMAP active-passive retrieval algorithm, removes the dependence on concurrent radar and radiometer observations, and thus can be applied to gap fill soil moisture at areas where the the SMAP active-passive retrieval algorithm is not able to. Compared with conventional one-layer machine learning models that directly downscale soil moisture from 9 km to 3 km, the two-layer framework avoids the dependence on the 9 km soil moisture that has additional uncertainties incurred by the indirect conversion from the 9 km brightness temperature. Moreover, it allows us to naturally introduce the average of historical (past 30 days) radar backscatter measurements as one of the key inputs to downscale the 9 km brightness temperature. This is useful as the vegetation and surface heterogeneity captured by the average of historical radar backscatter measurements can help produce more accurate downscaled brightness temperature, from which high resolution soil moisture with higher accuracy can be subsequently derived.

Note that the novelty of our proposed two-layer machine learning-based framework is that its design, including the structure and inputs, is motivated by the SMAP active-passive retrieval algorithm. Using the proposed framework, downscaled soil moisture that is highly consistent with the SMAP/Sentinel-1 3 km soil moisture product can be reconstructed at gap areas where the SMAP active-passive retrieval algorithm fails. The framework is a general one though that any machine learning algorithm can be embedded into it to downscale brightness temperature/soil moisture. We implement both a general one-layer model that directly downscales 9 km soil moisture to 3 km and our proposed two-layer framework under the transfer learning setting with the Random Forest algorithm [57] serving as the predictive model. The Random Forest model is specifically chosen here for its ability to handle complex non-linear relationships with reduced overfitting. It has also shown promising results in many soil moisture downscaling studies [44, 46, 58, 59]. The downscaled soil moisture produced by the Random Forest model through both the one-layer and the proposed two-layer frameworks are validated against the hold-out SMAP/Sentinel-1 retrieved 3 km soil moisture estimates at three regions with distinct climate regimes, Arizona, South Dakota, and Arkansas, during the growing season of 2018.

The contribution of this paper is threefold. First, it is the first study using machine learning to address the poor spatial and temporal coverage issue for downscaled soil moisture estimates that are retrieved by the radar-radiometer microwave combination approach. Second, it introduces the transfer learning strategy from machine learning field to enable knowledge learned between the SMAP/Sentinel-1 3 km product and the SMAP enhanced 9 km product over

large regional extent being transferred to spatially/temporally neighboring regions. Third, it designs a novel two-layer machine learning framework that is motivated by the original SMAP active-passive retrieval algorithm to improve the consistency between the machine learning model resulting predictions and the SMAP/Sentinel-1 3 km soil moisture. The average of historical radar backscatter measurements is introduced for the first time as one of the key inputs to machine learning models to aid capturing more subgrid heterogeneities. The rest of the paper is organized as follows. Section 2 describes the data sets and study area. The specifics of the methodology are presented in section 4. The results and validations are discussed in section 5. The conclusions and discussion for future work are then provided in section 6.

2 Data Sets and Study Area

2.1 Data Sets

The most recent SMAP/Sentinel-1 active-passive soil moisture product (L2_SM_SP) provides 3 km soil moisture and 3 km brightness temperature that can serve as the learning targets of our machine learning models. As a level 2 product, for any specific day, there are hundreds of data files each containing a sub-patch of the globally covered data. We generate daily composites from this level 2 product with the averaged value applied to overlapping estimates. We take the 9 km soil moisture and 9 km brightness temperature from the SMAP enhanced passive soil moisture product (L3_SM_P_E). For both the aforementioned SMAP soil moisture products, only the descending overpass, or local 6 am, data is used in this paper. These products are gridded using the Equal-Area Scalable Earth-2 (EASE2) projection [60] where the 3 km subgrids are nested consistently inside the 9 km grid. The grid configurations of the data are shown in Figure 2.
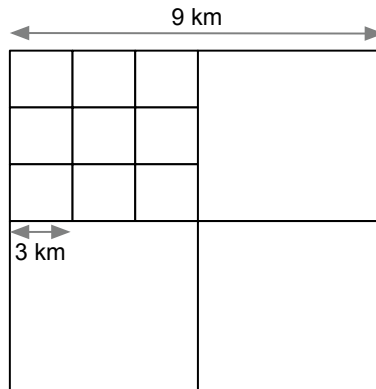

Figure 2: Nested EASE2 Grid at 9 km and 3 km supports.

We also take additional inputs to aid capturing the fine-scale heterogeneity in soil moisture and brightness temperature. Soil properties represented by the percent sand, percent clay, and bulk density were obtained from the Soil Geographic (STATSGO) Data Base [61]. The elevation data were obtained from the NASA Shuttle Radar Topography Mission Global 3 arc second product (SRTMGL3) [62]. Land surface controls represented by the land cover class, the leaf area index, and the land surface temperature were extracted from the MODIS products, MCD12Q1 [63], MCD15A3H [64], and MOD11A1 [65] respectively. Precipitation forcing data were obtained from the Global Precipitation Measurement [66] 3IMERGDF product. All these inputs were resampled to the 3-km EASE2-Grid projection through averaging (for inputs with resolutions higher than 3 km) or bilinear interpolation (for inputs with resolutions lower than 3 km) to match the grid size of the learning targets.

Additional post-processing was applied to land surface temperature and precipitation data. As retrieval for land surface temperature depends on the satellite thermal infrared channels, invalid surface temperature values are generated for surfaces that are obscured by clouds [67]. For these grids with invalid values, we search for historical values within a two-week finite window and select the most recent valid historical values as substitutes. For precipitation, to incorporate its lagged effect on vegetation, surface characteristics and soil moisture, instead of using the current-day precipitation values, we keep historical precipitation values from the most recent three days separately as inputs to the machine learning models.

2.2 Study Area

We apply the proposed framework at three US states with distinct climate regimes and land surface heterogeneities, Arizona, South Dakota, and Arkansas, separately (shown in Figure 3). Arizona has primarily an "arid" climate (BSk and BWh classification), South Dakota is classified as having a "fully humid" hydroclimate (Dfa classification) and Arkansas is "warm temperate" (Csc classification) according to the Köppen-Gieger classification [68]. While Arizona is predominantly composed of open shrublands (70.8%), South Dakota mainly consists of grasslands (56.4%) and croplands (40.6%) and Arkansas is covered with forest (28.7%), croplands (25.5%) and woody savannah (19%) [63]. Arizona has a high mean elevation (above mean sea level) of 1283.1 m while South Dakota and Arkansas have mean elevations of 663.2 m and 166.2 m respectively [62]. In Figure 3, we show daily examples of the 9 km and 3 km soil moisture. Arizona with the "arid-steppe-hot" climate generally have dry conditions compared with the other two states (see Figure 3(a) and 3(b)). Even with low soil moisture values, high levels of heterogeneity can still be seen at the 3 km resolution, especially for areas with latitude lower than 35°N. South Dakota and Arkansas have soil moisture values ranging from 0.0 cm^3/cm^3 to 0.5 cm^3/cm^3. While the high resolution soil moisture has more variability at Arkansas (Figure 3(e) and 3(f)), South Dakota is spatially homogeneous at 3 km (Figure 3(c) and 3(d)). The three study areas also observe different crop growth/vegetation activities during the growing season of 2018, as reflected by the temporal average of leaf area index shown in Figure 4.
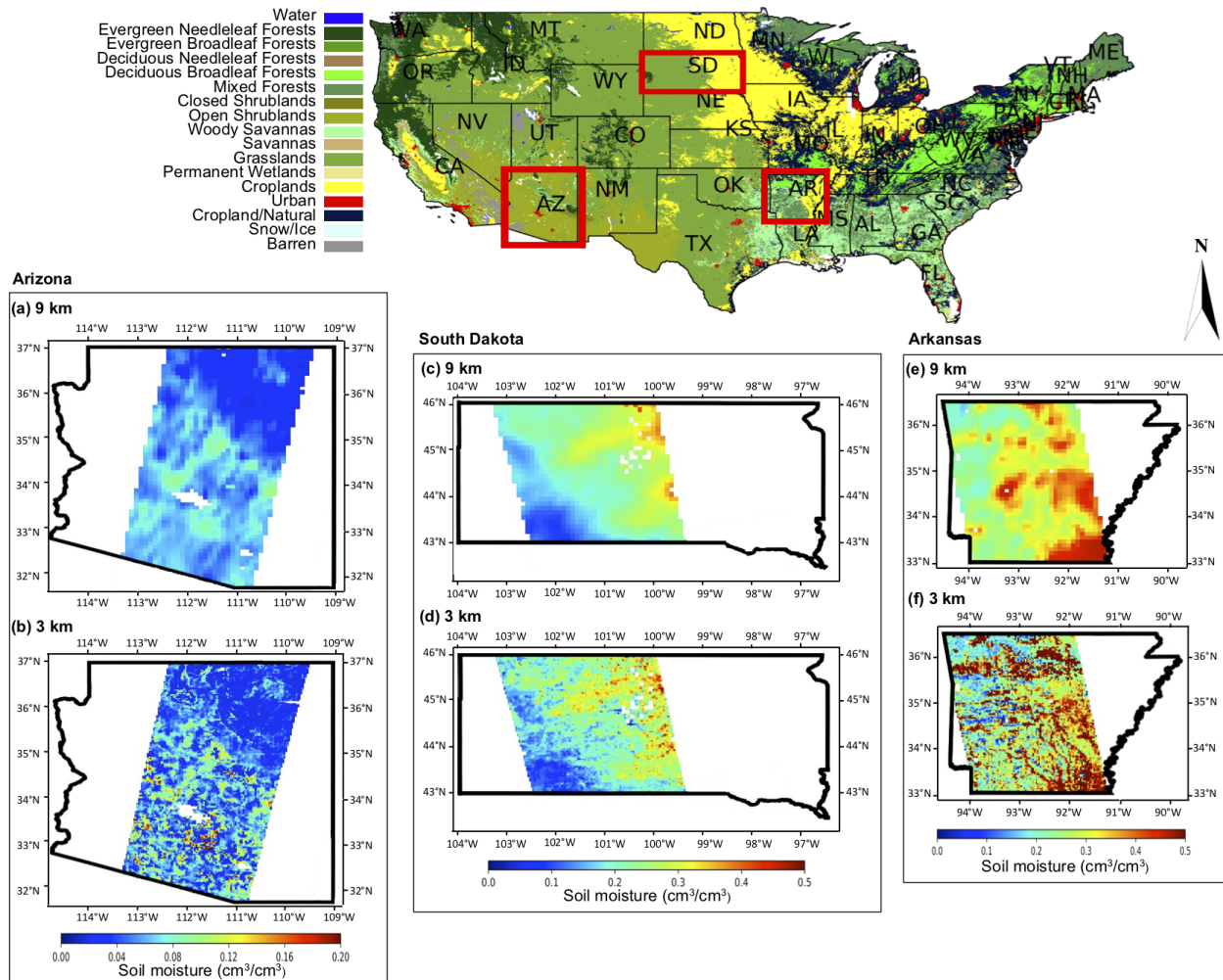

Figure 3: Locations of the three study areas. The background shows the MODIS IGBP land cover class. (a) 9 km soil moisture and (b) 3km soil moisture at Arizona on June 13th, 2018. (c) 9 km soil moisture and (d) 3 km soil moisture at South Dakota on June 12th, 2018. (e) 9 km soil moisture and (f) 3 km soil moisture at Arkansas on June 3th, 2018. 9 km soil moisture is converted from 9 km brightness temperature through the SCA algorithm while 3 km soil moisture is the downscaled product from the SMAP active-passive retrieval algorithm.

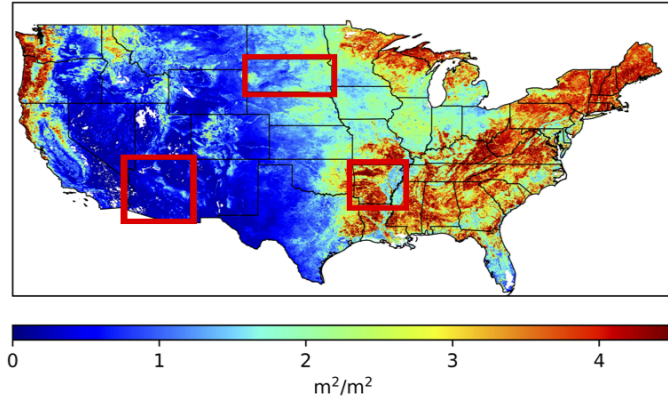Average Leaf Area Index from MCD15A3H (20180501 - 20180831)

Figure 4: Average of the leaf area index values between May 1, 2018 and August 31, 2018 from the MCD15A3H product.

3 The SMAP Active-Passive Retrieval Algorithm

We provide here an overview of the SMAP active-passive retrieval algorithm [28, 69] that motivates the design of our proposed two-layer machine learning-based framework. This algorithm adopts a two-layer retrieval strategy where the brightness temperature is downscaled first followed by soil moisture retrieval (Figure 5(a)).

(a) SMAP Active-Passive Retrieval Algorithm

current-day & historical 9 km brightness temperature from SMAP L3_SM_P_E

current-day & historical 3 km co-pol & cross-pol from SMAP L2_SM_SP

Brightness Temperature Downscaling

3 km brightness temperature

Single Channel Algorithm

3 km soil moisture

(b) One-layer Machine Learning Model

current-day 9 km soil moisture from SMAP L3_SM_P_E

$+ \mathcal{H}$ **Single-layer Machine Learning Model**

3 km soil moisture

$\mathcal{H}$ ancillary environmental variables including sand percentage, clay percentage, bulk density, elevation, precipitation, leaf area index, land surface temperature, landcover class, lat, lon

(c) Two-layer Machine Learning Framework

current-day 9 km brightness temperature from SMAP L3_SM_P_E

average & standard deviation of historical 3 km co-pol & cross-pol from SMAP L2_SM_SP

$+ \mathcal{H}$ **First-layer Machine Learning Model**

3 km brightness temperature

$+ \mathcal{H}$ **Second-layer Machine Learning Model**
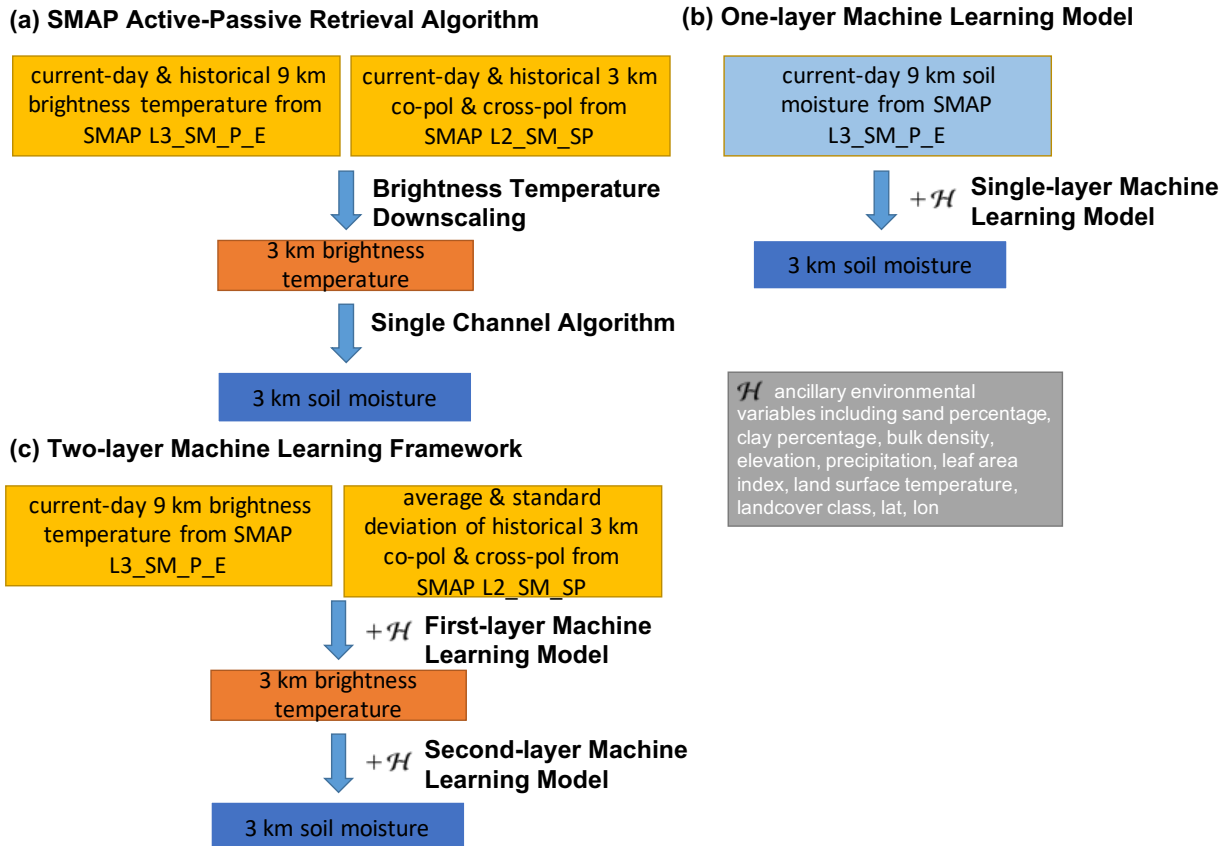
3 km soil moisture

Figure 5: Comparison of (a) the SMAP active-passive retrieval algorithm, (b) the one-layer machine learning model, and (c) the two-layer machine learning framework.

The SMAP active-passive retrieval algorithm first disaggregates the coarse-scale brightness temperature measurements (T_B, at polarization v or h) with the aid of fine-scale radar backscatter measurements. Both co-pol (σ_{vv} or σ_{hh}) and cross-pol (σ_{vh}) radar backscatter cross-section are used in the algorithm. Cross-pol measurements are included in the algorithm to capture the subgrid variations of brightness temperature within a coarse-scale footprint due to the variations in vegetation characteristics and surface roughness. The vegetation characteristics and surface roughness are assumed to be invariant within a short period of time. Suppose that we have brightness temperature measurements at a coarse support "C" and radar backscatter measurements at a fine support "F". Let the resolution of the downscaled soil moisture product be "M". Within a single pixel of the grid at support C, the disaggregated brightness temperature of a sub-pixel at support M can be obtained using

$$T_B(M) = T_B(C) + \beta(C) \cdot \{[\sigma_{vv}(M) - \sigma_{vv}(C)] + \Gamma \cdot [\sigma_{vh}(C) - \sigma_{vh}(M)]\}. \tag{1}$$

The parameters β and Γ here are derived from time-series radar ($\sigma_{vh}(C)$, $\sigma_{vv}(M)$, and $\sigma_{vh}(M)$) and radiometer observations ($T_B(C)$) within a short period of time, including the current day. Once the downscaled brightness temperature is obtained, the single channel algorithm (SCA) [29] is applied to retrieve the downscaled soil moisture.

Table 1 lists the inputs required for downscaling brightness temperature and SCA separately. For some of the derived inputs like $\sigma_{vv}(M)$, we also list their corresponding data sources that are directly retrieved by the microwave sensors. Parameters with t as superscript are time-series data retrieved within a finite moving window. Theoretical parameters like ω and τ depend on vegetation structures, polarization, microwave frequency, etc. They are currently obtained through a land cover-driven lookup table that contains parameter values under different land cover classes [70]. It can be seen from the table that the SMAP active-passive retrieval algorithm, especially the brightness temperature downscaling, requires concurrent radar and radiometer observations on the same day. The narrow imaging swath and low revisit schedule of the Sentinel radars thus severely restricts the spatial and temporal coverage of the resulting downscaled soil moisture estimates. In the next section, we propose a machine learning framework to account for this shortcoming.

Table 1: Inputs of the SMAP Active-Passive Retrieval Algorithm.

Brightness Temperature Downscaling	$T_B(C)$, $\sigma_{vv}(M), \sigma_{vv}(C) \leftarrow \sigma_{vv}(F)$, $\sigma_{vh}(M), \sigma_{vh}(C) \leftarrow \sigma_{vh}(F)$, $\beta(C) \leftarrow T_B^t(C), \sigma_{vv}^t(C)$, $\Gamma(C) \leftarrow \sigma_{vv}^t(M), \sigma_{vh}^t(M)$
Single Channel Algorithm	T_B, surface temperature, vegetation water content, sand & clay percentages theoretical parameters such as ω, τ land cover class

4 Methodology

4.1 Spatial-Temporal Transfer Learning

There are three hypotheses that we test in this paper: high resolution soil moisture/brightness temperature at gap areas can be reconstructed from the models learned at (1) spatial neighboring regions, (2) temporal neighboring regions, and (3) both spatial and temporal neighboring regions. We define these three settings as the spatial transfer learning, the temporal transfer learning, and the spatial-temporal transfer learning respectively. For the temporal transfer learning and the spatial-temporal transfer learning, a 30-day window is adopted to search for the most recent temporal neighboring regions for the gap regions. As shown in Figure 6, transfer learning models are built using data available at covered spatial and/or temporal neighboring regions (inside the orange frames) and are subsequently used to predict high-resolution soil moisture at the gap region (inside the red frame) where the original SMAP/Sentinel-1 active-passive soil moisture product is missing. The success of these transfer learning models depends on how effectively information learned at spatial/temporal neighboring regions can be extrapolated to the gap region.

The three transfer learning settings we define in this subsection enable expanded training data from regional-scale covered areas. Most of existing machine learning soil moisture downscaling methods use ground observed data from either catchment-scale campaigns whose generalization performance at various distinct climate regimes needs further verification, or spatially sparsely distributed soil moisture monitoring network that often incurs data scarcity issue for daily gap-filling/downscaling task. The expanded training data enabled by the transfer learning settings has the potential of learning more complex relationship between coarse-scale and fine-scale soil moisture and achieving
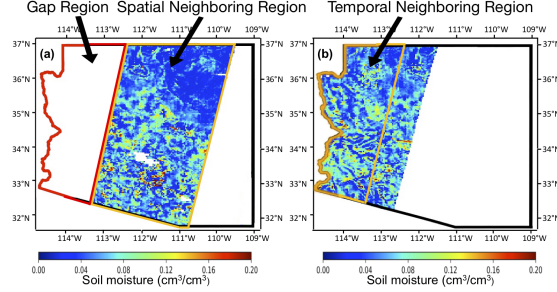
Figure 6: 3 km soil moisture swath at Arizona on (a) June 13, 2018 and (b) June 5th, 2018 from SMAP L2_SM_SP.

lower generalization errors at spatially/temporally neighboring regions. Additionally, when the estimates from the SMAP/Sentinel-1 3 km soil moisture product are used as target variables to train machine learning models, the knowledge transfer learning strategy has the advantage of maintaining high consistency between the gap-filled predictions and the SMAP/Sentinel-1 3 km product.

Note that we still focus on gap-filling the "neighboring" regions in this paper which fall into the same, or, at least, similar hydroclimates as the regions where the models are learned. Building models that can be applied to "almost everywhere" or discussing whether a model learned under one hydroclimate is applicable to another is beyond the scope of this paper and will be explored in the future.

4.2 Two-layer Machine Learning-based Framework

We discuss in this subsection the structure and inputs design of the transfer learning models. To downscale soil moisture that has a high consistency with the SMAP/Sentinel-1 3 km soil moisture estimates at gap areas, we hypothesize that it would be beneficial to learn two layered machine learning models whose structure and inputs design is guided by the SMAP active-passive retrieval algorithm.

First, we formulate the relationship learned by the first-layer machine learning model to disaggregate the 9 km brightness temperature to 3 km. Following the SMAP active-passive retrieval algorithm, we rewrite equation (1) as

$$T_B(3km) - T_B(9km) = \beta \cdot \{[\sigma_{vv}(3km) - \sigma_{vv}(9km)] + \Gamma \cdot [\sigma_{vh}(9km) - \sigma_{vh}(3km)]\}. \tag{2}$$

The left side of equation (2) can serve as the learning target of our first-layer machine learning model. It is available at areas where the radar and radiometer observations are available and missing at the gap areas where the radar observations are absent.

The parameters on the right side of equation (2) are restricted by the availability of radar observations and incur gap areas of the SMAP/Sentinel-1 3 km soil moisture product. To remove this dependence, we define the function that will be learned by our first-layer machine learning model as

$$y = T_B(3km) - T_B(9km) = f_1(rb^{hist}, \mathcal{H}). \tag{3}$$

Instead of directly using the radar observations $\sigma_{vv}(3km)$ and $\sigma_{vh}(3km)$ that are not available at gap areas, we introduce to our machine learning model the average of historical radar backscatter measurements within a 30-day window as substitutes to capture the subgrid heterogeneity in vegetation and surface physical characteristics. This substitution is based on the knowledge that radar backscatter measurements are introduced into the brightness temperature downscaling process to capture the subgrid heterogeneity and can be assumed to have less variability, compared with the dynamics of soil moisture, within a finite temporal window [28, 69]. To the best of our knowledge, this is the first time that the average of historical radar backscatter measurements is used as an input to machine learning models for soil moisture downscaling/gap-filling. In addition to the average, we also include the standard deviation of the historical 3 km radar backscatter measurements as an input to reflect the extent to which they change during the past 30 days.

This 30-day window to obtain the average/standard deviation of the historical radar backscatter measurements plus the aforementioned 30-day window for the search of temporal neighboring regions incur a 60-day set-up latency for our proposed method and the corresponding gap-filled 3 km soil moisture product. Once the 60-day set-up period has passed, the 3 km soil moisture can be produced in real-time at gap areas.

To adequately capture more soil moisture dynamics, we also use ancillary information such as soil properties, elevation, land surface controls, precipitation, latitude, and longitude. These environmental variables interact with soil moisture, vegetation, and surface characteristics [71, 72, 73, 74] and carry information of the fine-scale soil moisture heterogeneity

that we want to capture. Table 2 shows the inputs of our first-layer model. They can be decomposed into two parts: 1) the rb^{hist} set that includes the average/standard deviation of the historical radar backscatter measurements and 2) the $\mathcal{H}$ set that includes the auxiliary environmental variables.

Table 2: Inputs of the First-layer Machine Learning Model to Disaggregate the Brightness Temperature.

rb^{hist}	$mean(\sigma_{vv}(3km))^{hist}), mean(\sigma_{vh}(3km)^{hist}),$ $std(\sigma_{vv}(3km)^{hist}), std(\sigma_{vh}(3km)^{hist})$ $mean(\sigma_{vv}(9km))^{hist}), mean(\sigma_{vh}(9km)^{hist})$ $mean(\sigma_{vv}(3km))^{hist}) - mean(\sigma_{vv}(9km))^{hist}),$ $mean(\sigma_{vh}(3km))^{hist}) - mean(\sigma_{vh}(9km))^{hist})$
$\mathcal{H}$	sand percentage, clay percentage, bulk density, elevation, precipitation values in the past three days, leaf area index, land surface temperature, landcover class, lat, lon

Models will be trained at areas where the learning target and inputs are available. The learned model can then be used to obtain the predicted $\hat{y}$ at areas where $T_B(3km)$ is missing. We use the "hat" symbol over a variable to denote that it is a predicted value. The 3 km brightness temperature at these gap areas can, therefore, be reconstructed through

$$\hat{T}_B(3km) = T_B(9km) + \hat{y}. \tag{4}$$

After downscaling the 9 km brightness temperature, the downscaled 3 km soil moisture is obtained through the second-layer machine learning model given by

$$\widehat{SM}(3km) = f_2(\hat{T}_B(3km), \mathcal{H}). \tag{5}$$

Instead of relying on concurrent radar and radiometer observations and theoretical parameters as the SMAP active-passive retrieval algorithm, the proposed two-layer framework utilizes historical radar backscatter measurements and ancillary environmental information to capture high-resolution soil moisture dynamics. Once the models are learned at covered areas where both the 3 km estimates from the SMAP/Sentinel-1 product and the inputs are available, it can be applied to predict high-resolution soil moisture at gap areas where the SMAP active-passive retrieval algorithm fails.

In addition to the two-layer machine learning-based framework, we also implement a one-layer model whose performance is compared to our two-layer framework. The one-layer model directly downscales the soil moisture from 9 km to 3 km with the aid of available ancillary information. The function learned by this model can be written as:

$$SM(3km) = f_3(SM(9km), \mathcal{H}), \tag{6}$$

Figure 5(b) and (c) shows the structures of the one-layer model and the proposed two-layer machine learning-based framework respectively. Comparing Figure 5(a) and Figure 5(c), it can be seen that the two-layer machine learning-based framework follows a similar structure as the original SMAP/Sentinel active-passive retrieval algorithm while using a machine learning paradigm. Its performance over the one-layer model in terms of downscaling soil moisture at gap areas will be demonstrated through extensive machine learning-based experiments discussed in Section 5.

4.3 Random Forest Model

In this paper, the Random Forest model [57] is used for downscaling soil moisture/brightness temperature. Proposed in 2001, the Random Forest model quickly gained its reputation for being able to learn complex nonlinear relationships between the target variable and input features while resisting to the overfitting problem. Its superior performance is achieved through an ensemble of individually learned decision trees combined with the bagging method and random selections of features. During the training process of the Random Forest model, multiple hierarchical decision trees are learned independently with the goal of maximizing the variance reduction for each split. The individually grown decision trees can, however, easily suffer from the overfitting problem where significantly disparate performances can be observed on the training and test sets. To tackle this issue, the Random Forest model averages the predictions generated by all trees in the forest with additional strategies to reduce the correlation between them. The correlation reduction is done through tree bagging and the so-called "feature bagging". During the training process, each decision tree is exposed to different data subsets that are randomly sampled with replacement from the same training set. Additionally, "feature bagging" is adopted where randomly selected subset of the features are considered for each split. The Random Forest model generalizes well on test set when strong decision trees are constructed with controlled correlations between them.

5 Results and Discussions

We validate the downscaled soil moisture at three selected study areas, Arizona, South Dakota, and Arkansas, for the growing season of 2018 (May 1, 2018 - August 31, 2018). Data from March 1, 2018 to April 31, 2018 are also included for the temporal neighboring region search and for the generation of the average/standard deviation of the historical radar backscatter measurements. Besides the one-layer model (equation 6), we also compare the performance of our proposed two-layer framework with the 9 km soil moisture from the SMAP enhanced passive soil moisture product. We resample the 9 km soil moisture to 3 km by simply assuming that all the 3 km EASE2 subgrids inside one 9 km EASE2 grid have the same value. We denote this product as the "resampled 9 km soil moisture". The resampled 9 km soil moisture estimates serve as a reference for comparison with the one-layer and our proposed two-layer models. In terms of metrics, the correlation coefficient (R) and unbiased root mean square error (ubRMSE) are used to quantify and compare the overall agreement between the predicted 3 km soil moisture and the retrieved ones.

5.1 9 km versus One-layer Model versus Two-layer Framework

To demonstrate the performance of our proposed two-layer machine learning-based framework, we split the covered regions (where the 3 km soil moisture estimates are available) into training and test regions. Machine learning models learned at the training region are used to predict the downscaled soil moisture/brightness temperature at the test region. At each of the selected study areas, Arizona, South Dakota and Arkansas, there are $2 \sim 3$ different major swath patterns with $\sim$12 day interleaved revisit schedules. As shown in Figure 7, we select two swath patterns for each of the study areas, the main swath A and the shadow swath B. The overlap of the two swaths will be used as a filter to obtain the hold-out test region. For any specific day which has the main swath A available, the filter will be applied to obtain the test region (as shown in the red frames of Figure 7 (a), (c) and (e)), while the rest will be used as spatial neighboring regions for the training process (as shown in the orange frames in Figure 7 (a), (c) and (e)). For the temporal transfer learning task, a 30-day sliding window is adopted to search for the most recent shadow swath B. Once the most recent shadow swath B is obtained, the filter of the test region is applied to obtain the temporal neighboring region (as shown in the orange frames of Figure 7 (b), (d) and (f)).
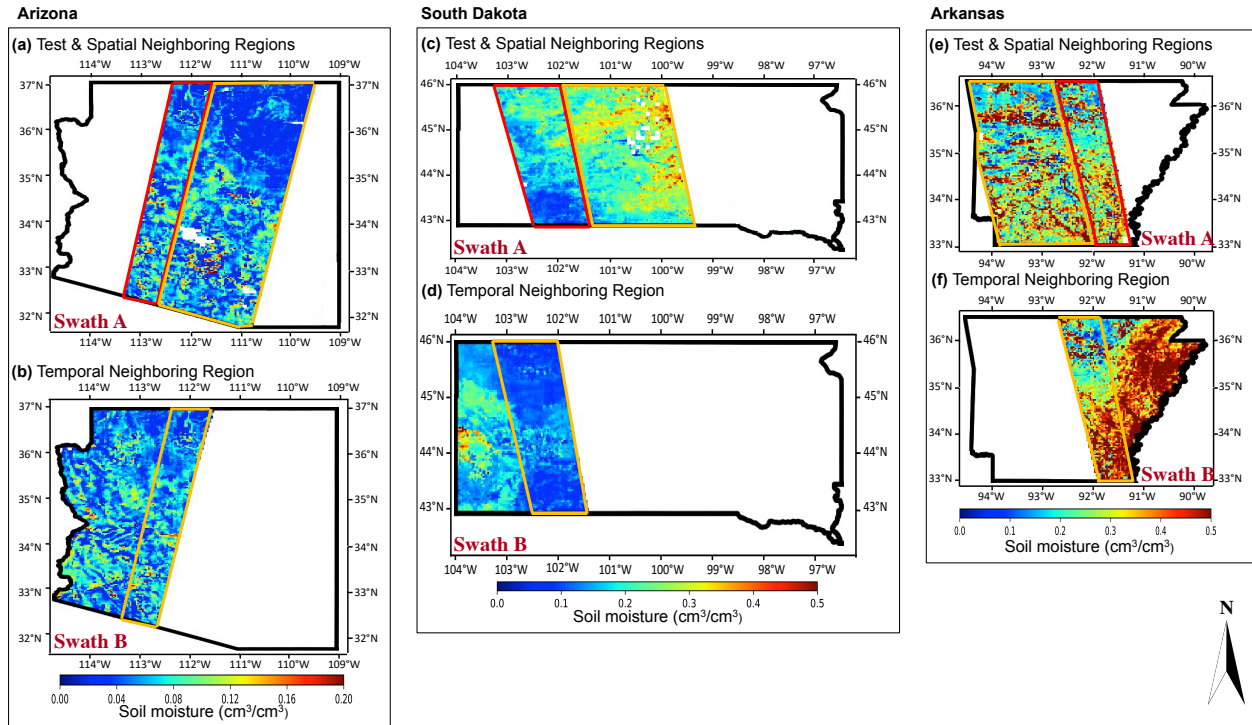

Figure 7: Train and test splits at Arizona, South Dakota and Arkansas. (a) selected swath A at Arizona on June 13th, 2018. (b) selected swath B at Arizona on June 5th, 2018. (c) selected swath A at South Dakota on July 17th, 2018. (d) selected swath B at South Dakota on July 11th, 2018. (e) selected swath A at Arkansas on July 8th, 2018. (f) selected swath B at Arkansas on June 21th, 2018.

This training and test splitting strategy mimics how the transfer learning is applied to fill/downscale soil moisture at real gap areas where the 3 km soil moisture estimates are indeed missing. It also allows us to compare the performance of the three transfer learning settings, the spatial transfer learning, temporal transfer learning, and the spatial-temporal transfer learning. Figure 8 shows, as an example, the test region at Arizona on June 13 and its corresponding spatial neighboring region and temporal neighboring region for the training. Table 3 lists the days of year (DOYs) at the selected study areas where the main swath A is available for test and spatial neighboring regions and the shadow swath B is available for a temporal neighboring regions search. Models are trained and predicted for each available test region and its corresponding training regions separately.
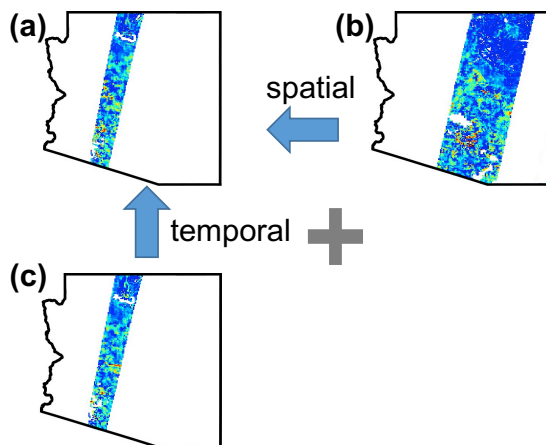
Figure 8: Spatial/temporal transfer learning for (a) test area at Arizona on June 13th, 2018. (b) spatial neighboring region on the same day. (c) search for temporal neighboring regions within 30-day sliding window is applied to obtain the most recent temporal neighboring region on June 5th, 2018.

Table 3: Days of Year (DOY) Data Were Available for Test, Spatial and Temporal Neighboring Regions between May 1, 2018 and August 31, 2018.

Region	Test & Spatial Neighboring Regions (DOY)	Temporal Neighboring Regions(DOY)
Arizona	127, 140, 151, 164, 188, 199, 212	95, 108, 119, 132, 143, 156, 167, 191, 204
South Dakota	126, 139, 150, 163, 187, 198, 211, 222, 235	107, 120, 144, 155, 168, 179, 192, 216, 227
Arkansas	130, 141, 154, 165, 189, 202, 213, 226, 237	100, 124, 148, 172, 197, 220

Figure 9 and Figure 10 compare the performance (in terms of R and ubRMSE respectively) of the resampled 9 km soil moisture, one-layer model and our proposed two-layer framework under different transfer learning settings at available test regions. At each selected study area, performance metrics of different DOYs are represented by boxplots to show a general pattern of how different models perform. It can be seen that the proposed two-layer framework generally outperforms both the resampled 9 km soil moisture product and the one-layer model in terms of R and ubRMSE under all three transfer learning settings.

The improvement in R is significant, especially at Arizona and Arkansas. Taking the spatial-temporal transfer learning as an example, the mean R at Arizona is increased to 0.723 for the two-layer framework compared to 0.532 for the one-layer model and 0.471 for the 9 km soil moisture, while the mean R at Arkansas is increased to 0.798 for the two-layer framework compared to 0.69 for the one-layer model and 0.523 for the 9 km soil moisture. Exceptions of improvement in performance are noticed at South Dakota for the spatial transfer learning and temporal transfer learning where relatively insignificant changes in the chosen metrics are found when comparing the resampled 9 km soil moisture product, the one-layer model, and our two-layer framework. This is, however, expected as the retrieved 3 km soil moisture has much lesser spatial heterogeneity compared with the 9 km soil moisture product at South Dakota as discussed in Subsection 2.2.

Focusing on the two-layer framework, Figure 9 also shows how different transfer learning settings perform, in terms of correlation coefficient, at the selected study areas. It can be seen that at Arizona and South Dakota, the temporal transfer learning achieves better performances (with mean R = 0.671 at Arizona and mean R = 0.797 at South Dakota) compared with the spatial transfer learning (with mean R = 0.585 at Arizona and mean R = 0.769 at South Dakota).
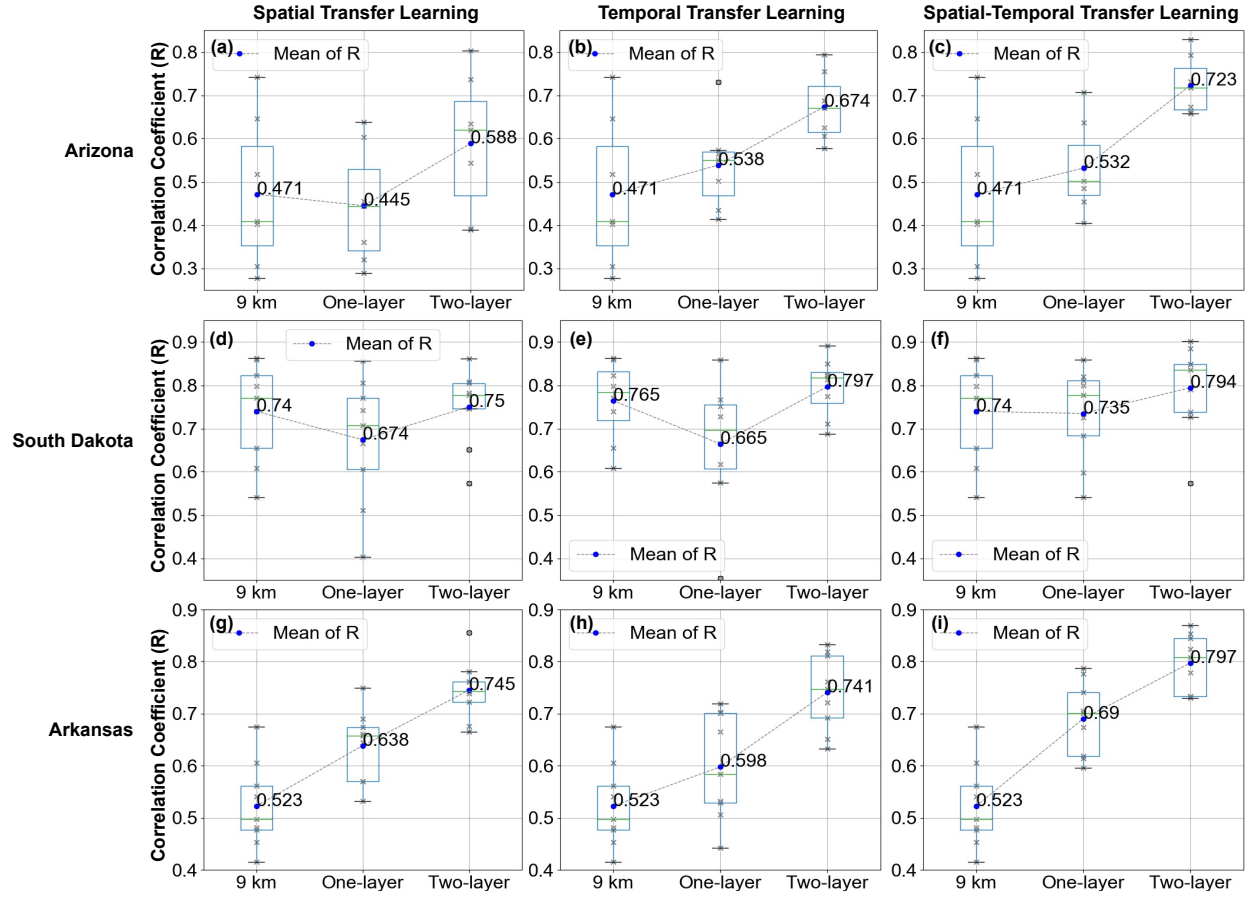
Figure 9: Correlation coefficient (R) comparisons of the resampled 9 km, one-layer model and our proposed two-layer framework for the selected study areas under different transfer learning settings.

While at Arkansas, the spatial transfer learning returns higher correlation coefficient (mean R = 0.741) compared with the temporal transfer learning (mean R = 0.733). One possible explanation is that Arkansas observes more vegetation cover as reflected in the higher average leaf area index (LAI) discussed in subsection 2.2. As the temporal transfer learning relies on the subgrid dynamics learned on a temporal neighboring region, having a dense vegetation cover will, as expected, impair its performance. For all the three study areas, the spatial-temporal transfer learning outperforms the spatial-only and temporal-only models. The mean R at Arizona, for example, is increased to 0.723 for the spatial-temporal transfer learning compared to 0.585 for the spatial transfer learning and 0.671 for the temporal transfer learning. The comparison of ubRMSE follows a similar pattern as R, we thus omit the discussion here.

To visually compare the performance of these models, Figure 11, as an example, focuses on a daily test region on June 13, 2018 at Arizona to show the disaggregated soil moisture produced by the resampled 9 km soil moisture product, the one-layer model and the proposed two-layer framework. It can be seen that although the one-layer model under the spatial-temporal transfer learning has the ability to reconstruct fine-scale soil moisture to some extent (Figure 11(c)), its downscaling quality is still inferior to the proposed two-layer framework, even to the one under the spatial transfer learning only (Figure 11(d)). With the proposed two-layer framework, more fine-scale soil moisture heterogeneities can be predicted/downscaled with improvement in both R and ubRMSE, especially under the spatial-temporal transfer learning setting (Figure 11(f)).

5.2 Transfer Learning Limitation Exploration

5.2.1 Spatial Transfer Learning

To compare the downscaling performances of different transfer learning settings, fixed-size test regions were adopted for the above experiments at each study area. Meanwhile it is worthwhile to continue exploring whether our proposed
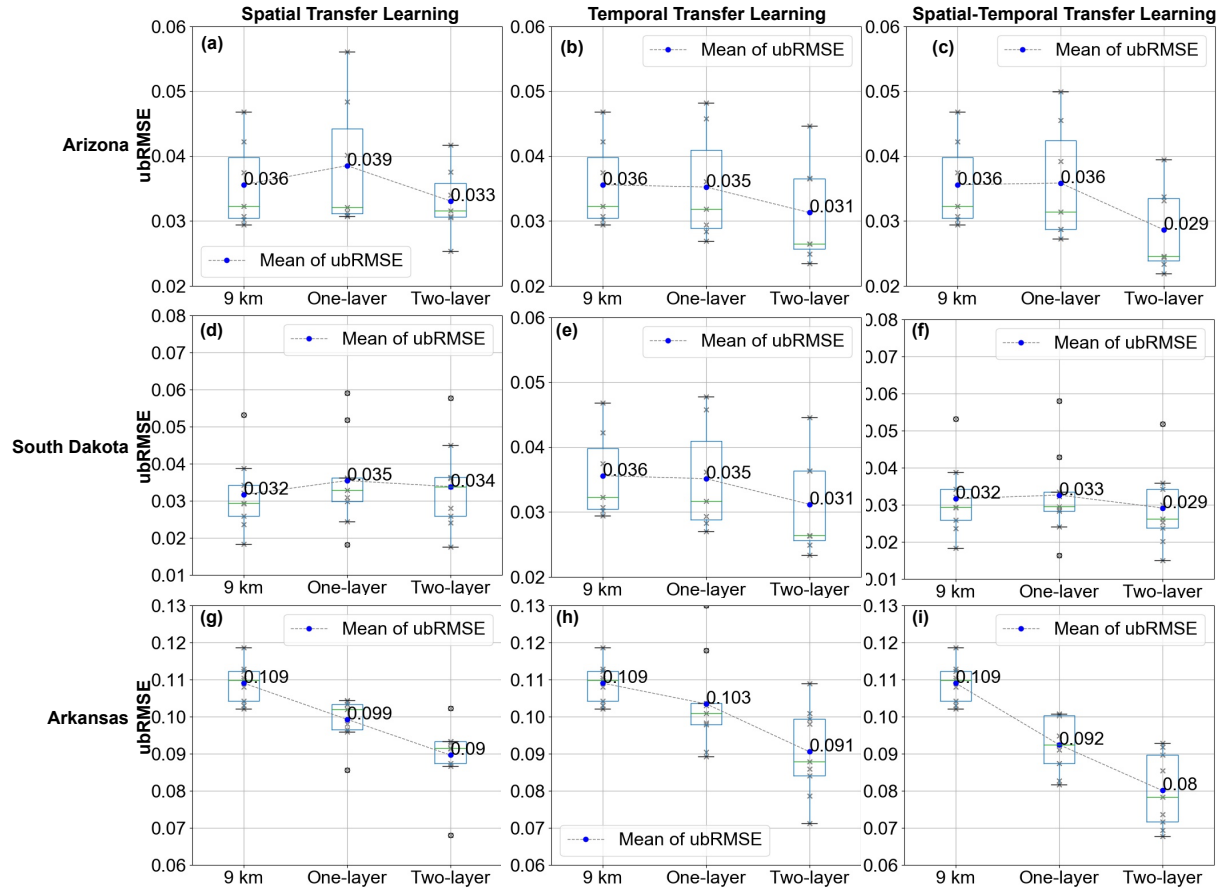
Figure 10: Unbiased RMSE (ubRMSE) comparisons of the resampled 9 km, one-layer model and our proposed two-layer framework for the selected study areas under different transfer learning settings.

two-layer framework can keep achieving satisfiable performance when the size of the test regions expands. To project how our models will perform when we fill the real gaps, or expand the observed regions, we split the training and test regions by shrinking the regions covered by the 3 km soil moisture. Taking the available swath at Arkansas on June 14th, 2018 as an example, as shown in Figure 12, we split the region covered by the SMAP/Sentinel-1 3 km soil moisture product (Figure 12 (a)) into training and test regions with various size ratio (Figure 12 (b), (c), (d) and (e)). Here, four different size ratios, 1: 4, 1: 2, 1: 1 and 2: 1, are chosen. A higher ratio indicates that less training samples are used during the training process and more samples are used to validate predictions. Models learned using data from the training region are used to downscale soil moisture at test region. Figure 13 shows the corresponding experiment results at the three selected study areas. While generally deteriorating performances were observed with the growing size ratio, at Arizona and Arkansas our proposed two-layer framework outperforms the resampled 9 km soil moisture and the one-layer model. Especially at Arkansas, the R values are approximately 0.7 when the test region is twice the size of the training region compared with ~ 0.4 R from the 9 km soil moisture and ~ 0.5 R from the one-layer model. In South Dakota, the two-layer framework, again as before, returns similar metrics as the 9 km soil moisture.

5.2.2 Temporal Transfer Learning

To obtain the temporal neighboring region for the temporal transfer learning and spatial-temporal transfer learning, we search back from the current day to find the most recent historical temporal neighboring region from another swath pattern within a 30-day window. In this subsection, we explore how the timespan between the current day test region and the obtained temporal neighboring region influences the predictive performance. For the Sentinel-1 radars, the temporal resolution of one swath pattern is ~ 12 days while the timespan between two different but consecutive swath patterns is ~ 6 days. Considering that the swaths may be missing due to various reasons, the timespan between the current-day test region and the obtained temporal neighboring region can be ~ 6 days, ~ 18 days or ~ 30 days. To explore how
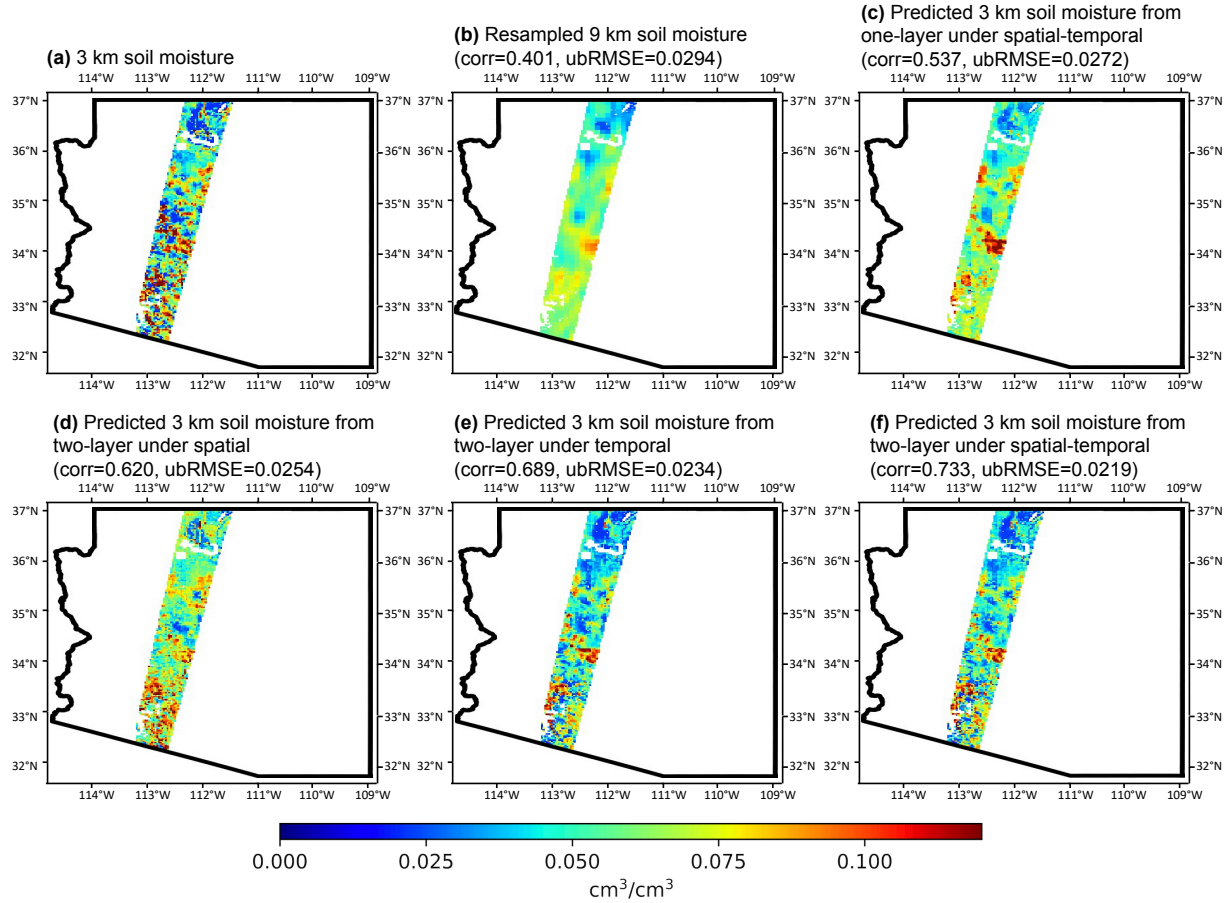
14

Figure 11: Performance comparisons for test region at Arizona on June 13th, 2018. (a) 3 km soil moisture from SMAP/Sentinel-1 active-passive Product. (b) resampled 9 km soil moisture from SMAP enhanced passive product. Predicted 3 km soil moisture from (c) the one-layer model under spatial-temporal transfer learning, (d) the two-layer framework under spatial transfer learning, (e) the two-layer framework under temporal transfer learning and (f) the two-layer framework under spatial-temporal transfer learning.

these different timespans influence the downscaling performances of the one-layer model and our two-layer framework, as shown in Figure 14, we continue searching within the 30-day window to find all available temporal neighboring regions and compare the experiment results aggregated by different timespans. Figure 15 shows the comparisons at the three study areas. All the three study areas observe deteriorating performances, to different extents, as the timespan increases between the test region and the temporal neighboring region. Again, our two-layer framework returns better downscaling performances, especially at Arizona and Arkansas, compared with the one-layer model and the resampled 9 km soil moisture.

5.3 Model Comparison

As stated before, the proposed two-layer framework is a general framework that any machine learning algorithm can be embedded in to accomplish the prediction task. In this section, we compare the performances of the Random Forest model with two other well-known models, the linear regression model and the XGBoost model [75]. The spatial-temporal transfer learning is considered here. It can be seen in Figure 16 that the linear regression model performs the worst compared with the other two non-linear models. This is expected as the relationships that we aim to capture using the machine learning models are non-linear based on the original theoretical algorithms of the SMAP active-passive product [69]. It can also be seen that our proposed two-layer framework outperforms the one-layer model for any of the three machine learning models.
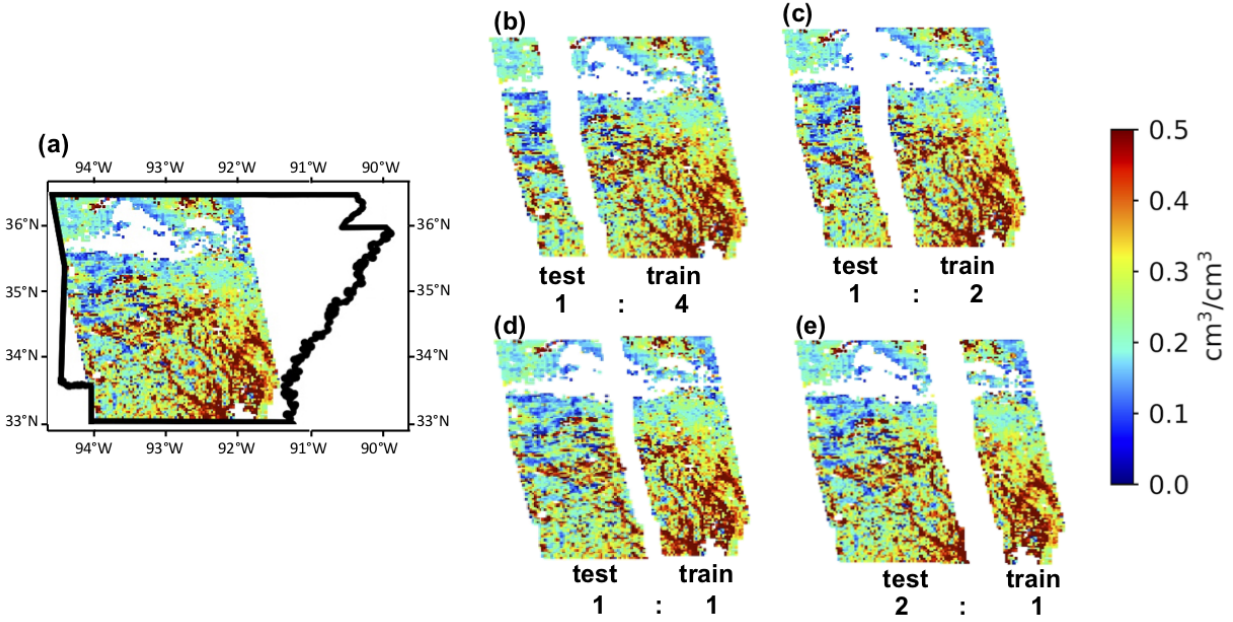
Figure 12: Vertical split of the whole swath at Arkansas on June 14th, 2018 with various size ratios of test region v.s. training region.
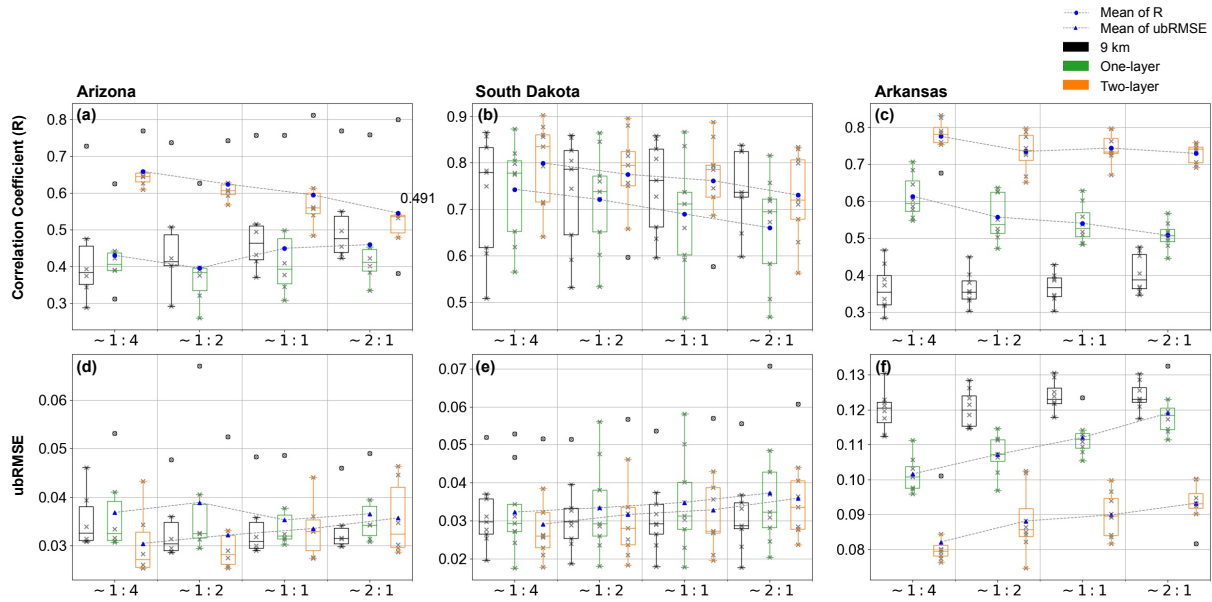

Figure 13: Performance comparisons of the resampled 9 km soil moisture, one-layer model and our proposed two-layer framework under different size ratios of the test region v.s. the training region.

5.4 Prediction at Gap Areas

In this subsection, we predict and compare the downscaled soil moisture produced by the models at real gap areas where the 3 km soil moisture estimates are indeed missing in the SMAP/Sentinel-1 active passive product. As we have discussed in Subsection 4.1, we first train models using data from spatial-temporal neighboring regions of the gap regions. The learned models are then fitted to predict the 3 km brightness temperature and soil moisture at real gap areas. Figure 17 shows the predicted high resolution soil moisture at Arizona on June 13th, 2018, as an example, from the resampled 9 km soil moisture, the one-layer model and the two-layer framework under different transfer learning
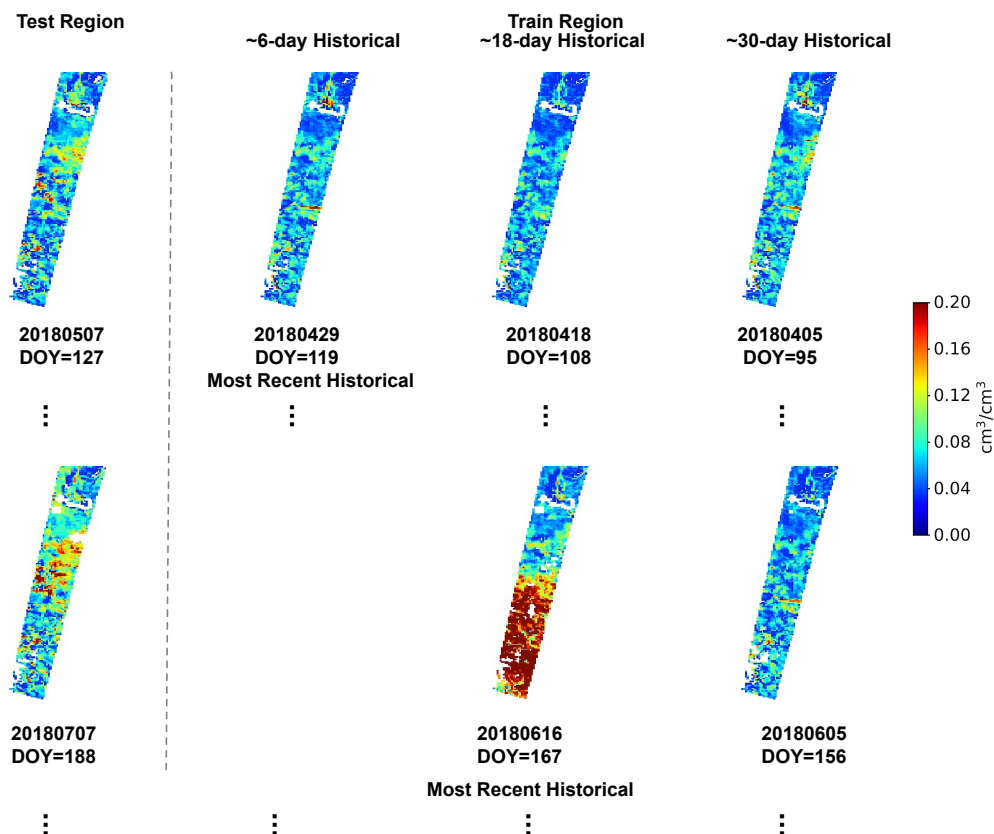
Figure 14: Search for temporal neighboring regions within a 30-day window for test regions at Arizona on May 7th, 2018 and July 7th, 2018.

settings. Again, our two-layer framework reconstructs more subgrid soil moisture heterogeneities compared with the one-layer model.

Gaps of SMAP/Sentinel-1 active-passive product for continental United States can be filled adopting the same methodology. The produced gap-filled soil moisture has the same 3 km resolution as the SMAP/Sentinel-1 active-passive product and the same spatial and temporal coverage as the SMAP enhanced passive product. Figure 18 (a) and (b) show the daily 3 km soil moisture product from the SMAP/Sentinel-1 active passive product and daily resampled 9 km soil moisture product from the SMAP enhanced passive product, on June 17th, 2018, respectively. Large areas that are not covered by the fine-scale soil moisture can be observed. Again, this is due to missing high resolution radar backscatter measurements. Figure 18 (c) and (d) show the comparison of the gap-filled soil moisture produced by the one-layer model and our proposed two-layer framework. We were able to gap-fill most of the missing areas except those that have missing inputs, mainly the historical radar scatter measurements. Additionally, while the one-layer model is able to reconstruct the 3 km soil moisture as our two-layer framework (under the spatial-temporal transfer learning), it produces much less fine-scale soil moisture heterogeneities as our proposed framework.

6   Conclusions

Recognizing the importance of global-scale soil moisture estimates with fine spatial and temporal resolution, this paper introduces the transfer learning strategy for the first time to enable regional gap-filled high-resolution soil moisture that maintains high consistency with the SMAP/Sentinel-1 3 km soil moisture product. It also presents a novel two-layer machine learning-based framework motivated by the SMAP active-passive retrieval algorithm. The two-layer framework can downscale/gap-fill soil moisture with more heterogeneity captured at areas where the SMAP/Sentinel-1 active-passive 3 km soil moisture product is missing. The average of historical radar backscatter measurements is introduced for the first time as one of the key inputs to machine learning models for soil moisture downscaling. We compare the two-layer framework with a conventional one-layer model and the resampled 9 km soil moisture product
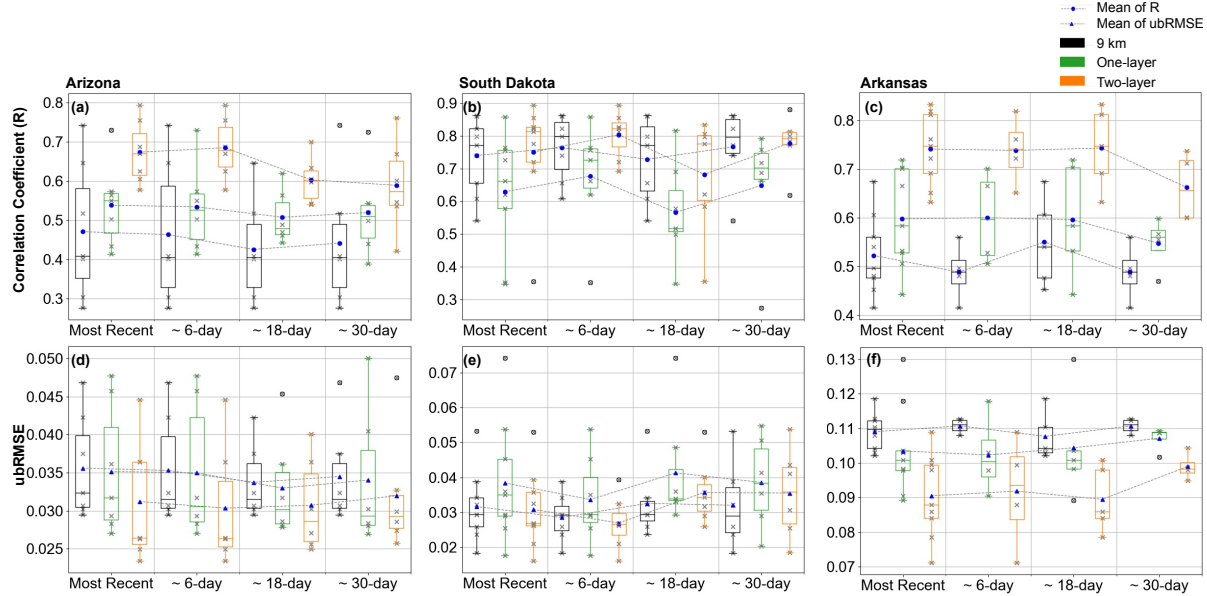
17

Figure 15: Performance comparisons of the resampled 9 km soil moisture, one-layer model and our proposed two-layer framework under different temporal distances between the test region and the temporal neighboring region.
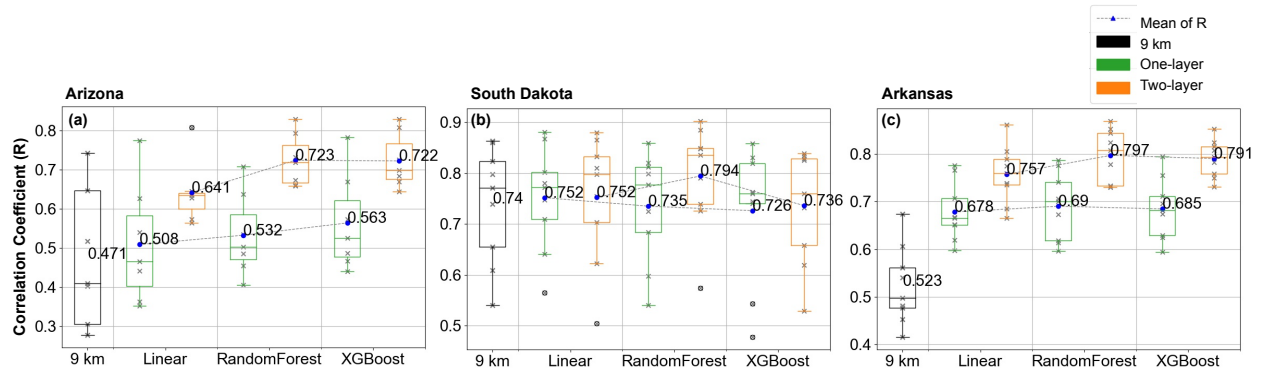

Figure 16: Performance comparisons of the linear regression, Random Forest and XGBoost models under the spatial-temporal transfer learning setting at (a) Arizona, (b) South Dakota and (c) Arkansas.

under three different transfer learning settings against hold-out SMAP/Sentinel-1 active-passive soil moisture estimates. We show that our two-layer framework outperforms the one-layer model and the resampled 9 km soil moisture, in terms of R and ubRMSE, under all scenarios. The most significant performance improvements of the proposed two-layer framework were seen on the R under the spatial-temporal transfer learning where it is increased to 0.723 at Arizona compared to 0.471 for the resampled 9 km and 0.532 for the one-layer, 0.82 at South Dakota compared to 0.765 for the resampled 9 km and 0.76 for the one-layer, and 0.798 at Arkansas compared to 0.523 for the resampled 9 km and 0.69 for the one-layer. Another benefit of the two-layer machine learning-based framework is that it also produces downscaled brightness temperature at gap areas as an intermediate product. The downscaled brightness temperature with improved spatial and temporal coverage is also useful and has been applied to various data assimilation applications, such as the SMAP Level 4 product [76].

One limitation of our gap-filled soil moisture product is that its availability is still restricted by the availability of the inputs, mainly the 9 km soil moisture and 9 km brightness temperature from the SMAP enhanced passive product. The best temporal resolution produced is therefore ∼2-3 days. This issue will hopefully be addressed by the generation of seamlessly covered coarse-scale soil moisture and/or brightness temperature data in the future.This can be achieved by the development of another gap-filling technique to fill the gaps of the 9 km soil moisture product or a fusion of multiple passive microwave soil moisture products.
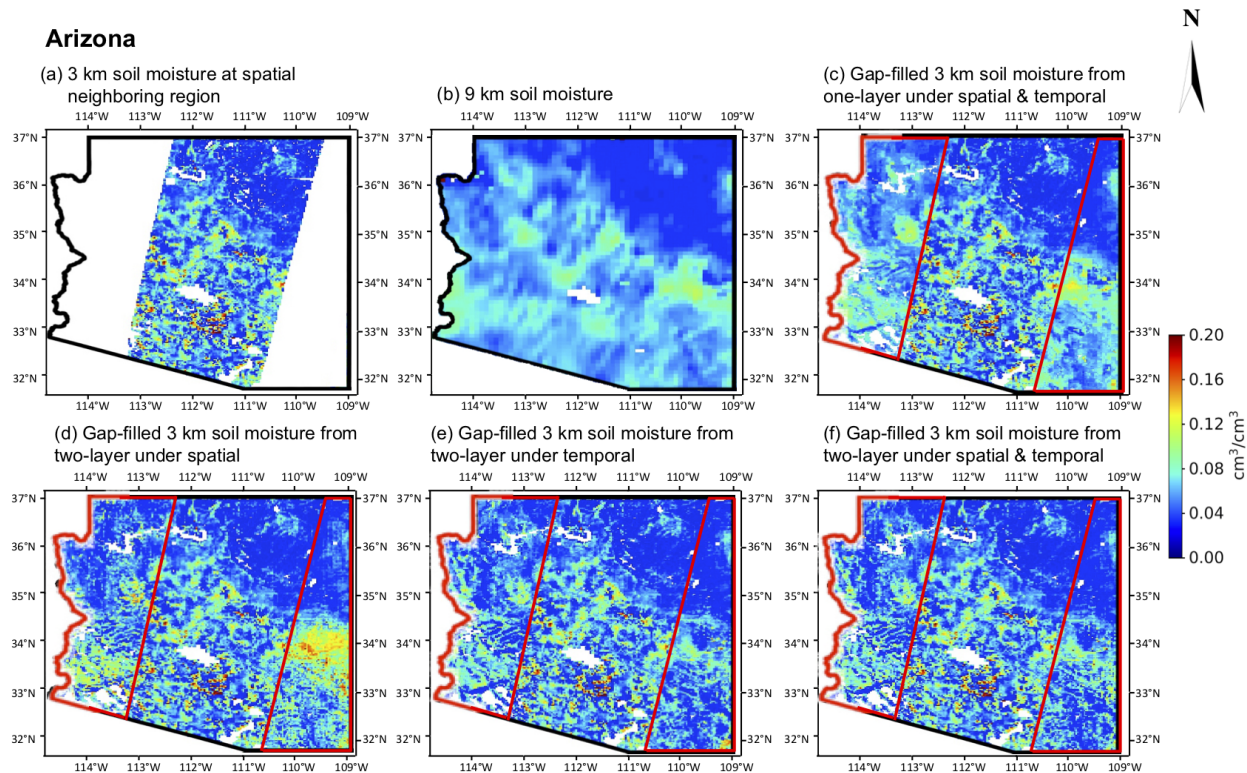
Figure 17: Real gap filling at Arizona on June 13th, 2018. (a) 3 km soil moisture from SMAP/Sentinel Product for spatial neighboring region on the same day. (b) Resampled 9 km soil moisture from SMAP L3_SM_P_E. Gap-filled 3 km soil moisture from (c) the one-layer model using spatial-temporal transfer learning, (d) the hierarchical learning models using spatial transfer learning, (e) the hierarchical learning models using temporal transfer learning and (f) the hierarchical learning models using spatial-temporal transfer learning.

References

[1] John D. Bolten, Wade T. Crow, Xiwu Zhan, Thomas J. Jackson, and Curt A. Reynolds. Evaluating the utility of remotely sensed soil moisture retrievals for operational agricultural drought monitoring. *IEEE J. Sel. Top. Appl. Earth Observations Remote Sensing*, 3(1):57–66, March 2010.

[2] M. Drusch. Initializing numerical weather prediction models with satellite-derived surface soil moisture: Data assimilation experiments with ECMWF's integrated forecast system and the TMI soil moisture data set. *J. Geophys. Res.*, 112(D3), February 2007.

[3] Sonia I. Seneviratne, Thierry Corti, Edouard L. Davin, Martin Hirschi, Eric B. Jaeger, Irene Lehner, Boris Orlowsky, and Adriaan J. Teuling. Investigating soil moisture–climate interactions in a changing climate: A review. *Earth-Science Reviews*, 99(3-4):125–161, May 2010.

[4] John Pastor and W. M. Post. Influence of climate, soil moisture, and succession on forest carbon and nitrogen cycles. *Biogeochemistry*, 2(1):3–27, March 1986.

[5] Wenju Cai, Tim Cowan, Peter Briggs, and Michael Raupach. Rising temperature depletes soil moisture and exacerbates severe drought conditions across southeast australia. *Geophys. Res. Lett.*, 36(21), November 2009.

[6] N. Wanders, D. Karssenberg, A. de Roo, S. M. de Jong, and M. F. P. Bierkens. The suitability of remotely sensed soil moisture for improving operational flood forecasting. *Hydrol. Earth Syst. Sci.*, 18(6):2343–2357, June 2014.

[7] H.R. Bogena, J.A. Huisman, C. Oberdörster, and H. Vereecken. Evaluation of a low-cost soil water content sensor for wireless network applications. *J Hydrol (Amst)*, 344(1-2):32–42, September 2007.

[8] D. A. Robinson, S. B. Jones, J. M. Wraith, D. Or, and S. P. Friedman. A review of advances in dielectric and electrical conductivity measurement in soils using time domain reflectometry. *Vadose Zone Journal*, 2(4):444, 2003.
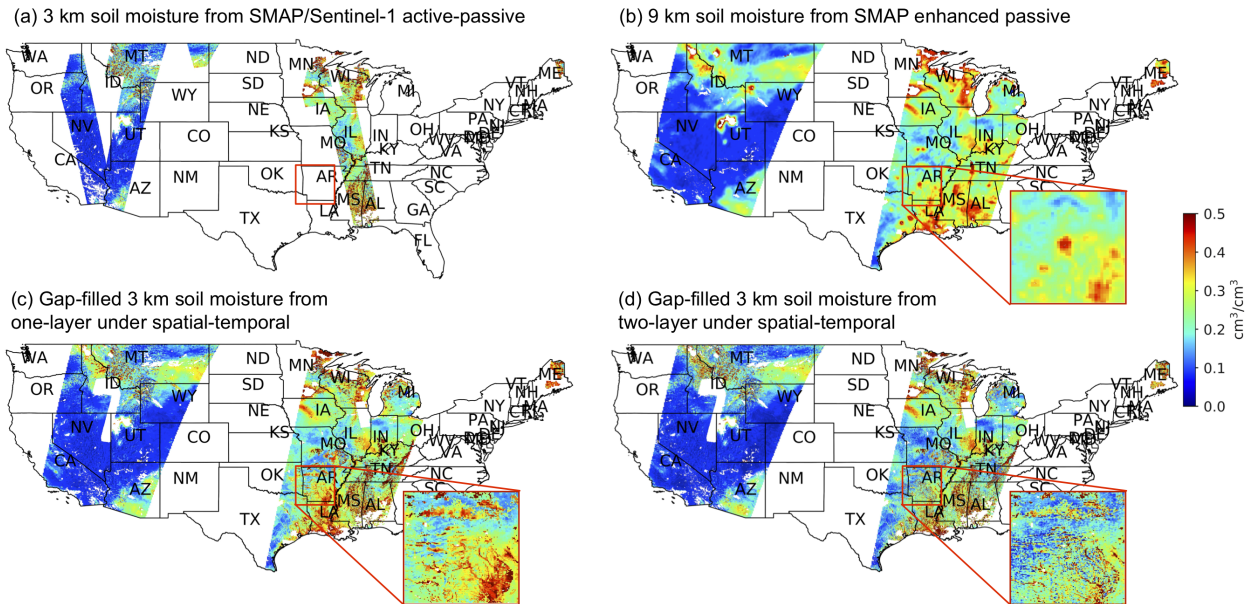
Figure 18: Real gap filling of the Continental United States on June 16th, 2018. (a) Observed 3 km soil moisture from SMAP L2_SM_SP. (b) Resampled 9 km soil moisture from SMAP L3_SM_P_E. (c) Gap-filled 3 km soil moisture from the one-layer model under the spatial-temporal transfer learning setting. (d) Gap-filled 3 km soil moisture from the proposed theory-guided hierarchical framework under the spatial-temporal transfer learning setting.

[9] Alan Robock, Konstantin Y. Vinnikov, Govindarajalu Srinivasan, Jared K. Entin, Steven E. Hollinger, Nina A. Speranskaya, Suxia Liu, and A. Namkhai. The global soil moisture data bank. *Bull. Am. Meteorol. Soc.*, 81(6):1281–1299, 2000.

[10] Wolfgang Wagner, Sebastian Hahn, Richard Kidd, Thomas Melzer, Zoltan Bartalis, Stefan Hasenauer, Julia Figa-Saldaña, Patricia de Rosnay, Alexander Jann, Stefan Schneider, Jürgen Komma, Gerhard Kubu, Katharina Brugger, Christoph Aubrecht, Johann Züger, Ute Gangkofner, Stefan Kienberger, Luca Brocca, Yong Wang, Günter Blöschl, Josef Eitzinger, and Kla Steinnocher. The ASCAT soil moisture product: A review of its specifications, validation results, and emerging applications. *Meteorol. Z.*, 22(1):5–33, February 2013.

[11] E G Njoku, T J Jackson, V Lakshmi, T K Chan, and S V Nghiem. Soil moisture retrieval from AMSR-e. *IEEE Trans. Geosci. Remote Sensing*, 41(2):215–229, February 2003.

[12] Yann H Kerr, Philippe Waldteufel, Jean-Pierre Wigneron, Steven Delwart, François Cabot, Jacqueline Boutin, Maria-José Escorihuela, Jordi Font, Nicolas Reul, Claire Gruhier, Silvia Enache Juglea, Mark R Drinkwater, Achim Hahne, Manuel Martín-Neira, and Susanne Mecklenburg. The SMOS mission: New tool for monitoring key elements ofthe global water cycle. *Proc. IEEE*, 98(5):666–687, May 2010.

[13] Dara Entekhabi, Eni G. Njoku, Peggy E. O'Neill, Kent H. Kellogg, Wade T. Crow, Wendy N. Edelstein, Jared K. Entin, Shawn D. Goodman, Thomas J. Jackson, Joel Johnson, John Kimball, Jeffrey R. Piepmeier, Randal D. Koster, Neil Martin, Kyle C. McDonald, Mahta Moghaddam, Susan Moran, Rolf Reichle, J. C. Shi, Michael W. Spencer, Samuel W. Thurman, Leung Tsang, and Jakob Van Zyl. The soil moisture active passive (SMAP) mission. *Proc. IEEE*, 98(5):704–716, May 2010.

[14] Ramon Torres, Paul Snoeij, Dirk Geudtner, David Bibby, Malcolm Davidson, Evert Attema, Pierre Potin, BjÖrn Rommen, Nicolas Floury, Mike Brown, Ignacio Navas Traver, Patrick Deghaye, Berthyl Duesmann, Betlem Rosich, Nuno Miranda, Claudio Bruno, Michelangelo L'Abbate, Renato Croci, Andrea Pietropaolo, Markus Huchler, and Friedhelm Rostan. GMES sentinel-1 mission. *Remote Sensing of Environment*, 120:9–24, May 2012.

[15] A. AghaKouchak, A. Farahmand, F. S. Melton, J. Teixeira, M. C. Anderson, B. D. Wardlow, and C. R. Hain. Remote sensing of drought: Progress, challenges and opportunities. *Rev. Geophys.*, 53(2):452–480, June 2015.

[16] Randal D Koster, Luca Brocca, Wade T Crow, Mariko S Burgin, and Gabrielle J M De Lannoy. Precipitation estimation using l-band and c-band soil moisture retrievals. *Water Resour Res*, 52(9):7213–7225, September 2016.

[17] Siyuan Tian, Paul Tregoning, Luigi J. Renzullo, Albert I. J. M. van Dijk, Jeffrey P. Walker, Valentijn R. N. Pauwels, and Sébastien Allgeyer. Improved water balance component estimates through joint assimilation of GRACE water storage and SMOS soil moisture retrievals. *Water Resour Res*, 53(3):1820–1840, March 2017.

[18] E G Njoku, W J Wilson, S H Yueh, S J Dinardo, F K Li, T.J. Jackson, V. Lakshmi, and J. Bolten. Observations of soil moisture using a passive and active low-frequency microwave airborne sensor during SGP99. *IEEE Trans. Geosci. Remote Sensing*, 40(12):2659–2673, December 2002.

[19] Fawwaz T. Ulaby, Pascale C. Dubois, and Jakob van Zyl. Radar mapping of surface soil moisture. *J Hydrol (Amst)*, 184(1-2):57–84, October 1996.

[20] E G Njoku and Dara Entekhabi. Passive microwave remote sensing of soil moisture. *J Hydrol (Amst)*, 184(1-2):101–129, October 1996.

[21] P E O'Neill, S Chan, E G Njoku, T Jackson, and R Bindlish. SMAP L3 radiometer global daily 36 km EASE-grid soil moisture, version 5, 2018a.

[22] P E O'Neill, S Chan, E G Njoku, T Jackson, and R Bindlish. SMAP enhanced L3 radiometer global daily 9 km EASE-grid soil moisture, version 2, 2018b.

[23] Jianzhi Dong and Wade T. Crow. The added value of assimilating remotely sensed soil moisture for estimating summertime soil moisture - air temperature coupling strength. *Water Resour Res*, July 2018.

[24] Yang Lu, Susan C. Steele-Dunne, Leila Farhadi, and Nick van de Giesen. Mapping surface heat fluxes by assimilating SMAP soil moisture and GOES land surface temperature data. *Water Resour Res*, December 2017.

[25] R. C. Nijzink, S. Almeida, I. G. Pechlivanidis, R. Capell, D. Gustafssons, B. Arheimer, J. Parajka, J. Freer, D. Han, T. Wagener, R. R. P. Nooijen, H. H. G. Savenije, and M. Hrachowitz. Constraining conceptual hydrological models with multiple information sources. *Water Resour Res*, 54(10):8332–8362, October 2018.

[26] Jian Peng, Alexander Loew, Olivier Merlin, and Niko E. C. Verhoest. A review of spatial downscaling of satellite remotely sensed soil moisture. *Rev. Geophys.*, 55(2):341–366, June 2017.

[27] Sabah Sabaghy, Jeffrey P. Walker, Luigi J. Renzullo, and Thomas J. Jackson. Spatially enhanced passive microwave derived soil moisture: Capabilities and opportunities. *Remote Sensing of Environment*, 209:551–580, May 2018.

[28] N N Das, Dara Entekhabi, Eni G. Njoku, Jiancheng J. C. Shi, Joel T. Johnson, and Andreas Colliander. Tests of the SMAP combined radar and radiometer algorithm using airborne field campaign observations and simulated data. *IEEE Trans. Geosci. Remote Sensing*, 52(4):2018–2028, April 2014.

[29] Thomas J. Jackson. III. measuring surface soil moisture using passive microwave remote sensing. *Hydrol Process*, 7(2):139–152, April 1993.

[30] D Entekhabi, N Das, E Njoku, J Johnson, and J Shi. SMAP L3 radar/radiometer global daily 9 km EASE-grid soil moisture, version 3, 2016.

[31] N. N. Das, D. Entekhabi, S. Kim, S. Yueh, and P. O'Neill. Combining SMAP and sentinel data for high-resolution soil moisture product. In *2016 IEEE International Geoscience and Remote Sensing Symposium (IGARSS)*, pages 129–131. IEEE, July 2016.

[32] Simon Yueh, Dara Entekhabi, Peggy O'Neill, Eni Njoku, and Jared Entin. NASA soil moisture active passive mission status and science performance. In *2016 IEEE International Geoscience and Remote Sensing Symposium (IGARSS)*, pages 116–119. IEEE, July 2016.

[33] H Lievens, R H Reichle, Q Liu, G J M De Lannoy, R S Dunbar, S B Kim, N N Das, M Cosh, J P Walker, and W Wagner. Joint sentinel-1 and SMAP data assimilation to improve soil moisture estimates. *Geophys Res Lett*, 44(12):6145–6153, June 2017.

[34] E. Santi, S. Paloscia, S. Pettinato, D. Entekhabi, S. H. Alemohammad, and A. G. Konings. Integration of passive and active microwave data from SMAP, AMSR2 and sentinel-1 for soil moisture monitoring. In *2016 IEEE International Geoscience and Remote Sensing Symposium (IGARSS)*, pages 5252–5255. IEEE, July 2016.

[35] C. Rudiger, C.-H. Su, D. Ryu, and W. Wagner. Disaggregation of low-resolution l-band radiometry using c-band radar data. *IEEE Geosci. Remote Sensing Lett.*, 13(10):1425–1429, October 2016.

[36] N N Das, D Entekhabi, R S Dunbar, S Kim, S Yueh, A Colliander, P E O'Neill, and T Jackson. SMAP/Sentinel-1 L2 radiometer/radar 30-second scene 3 km EASE-grid soil moisture, version 2, 2018.

[37] European Space Agency. Sentinel-1 User Handbook. Technical report, 2013.

[38] Jeffrey P. Walker and Paul R. Houser. Requirements of a global near-surface soil moisture satellite mission: accuracy, repeat time, and spatial resolution. *Adv Water Resour*, 27(8):785–801, August 2004.

[39] N. S. Chauhan, S. Miller, and P. Ardanuy. Spaceborne soil moisture estimation at high resolution: a microwave-optical/IR synergistic approach. *Int J Remote Sens*, 24(22):4599–4622, January 2003.

[40] Olivier Merlin, Christoph Rudiger, Ahmad Al Bitar, Philippe Richaume, Jeffrey P. Walker, and Yann H. Kerr. Disaggregation of SMOS soil moisture in southeastern australia. *IEEE Trans. Geosci. Remote Sensing*, 50(5):1556–1571, May 2012.

[41] María Piles, Adriano Camps, Mercè Vall-llossera, Ignasi Corbella, Rocco Panciera, Christoph Rudiger, Yann H. Kerr, and Jeffrey Walker. Downscaling SMOS-derived soil moisture using MODIS visible/infrared data. *IEEE Trans. Geosci. Remote Sensing*, 49(9):3156–3166, September 2011.

[42] H. Lievens, S.K. Tomer, A. Al Bitar, G.J.M. De Lannoy, M. Drusch, G. Dumedah, H.-J. Hendricks Franssen, Y.H. Kerr, B. Martens, M. Pan, J.K. Roundy, H. Vereecken, J.P. Walker, E.F. Wood, N.E.C. Verhoest, and V.R.N. Pauwels. SMOS soil moisture assimilation for improved hydrologic simulation in the murray darling basin, australia. *Remote Sensing of Environment*, 168:146–162, October 2015.

[43] Rolf H. Reichle, Dara Entekhabi, and Dennis B. McLaughlin. Downscaling of radio brightness measurements for soil moisture estimation: A four-dimensional variational data assimilation approach. *Water Resour Res*, 37(9):2353–2364, September 2001.

[44] Peyman Abbaszadeh, Hamid Moradkhani, and Xiwu Zhan. Downscaling SMAP radiometer soil moisture over the CONUS using an ensemble learning method. *Water Resour Res*, December 2018.

[45] S. Chai, J. Walker, Bert Veenendaal, and Geoff West. An artificial neural network model for downscaling of passive microwave soil moisture. *Recent Researches in Hydrology, Geology and Continuum Mechanics*, 2011.

[46] Jungho Im, Seonyoung Park, Jinyoung Rhee, Jongjin Baik, and Minha Choi. Downscaling of AMSR-e soil moisture with MODIS products using machine learning approaches. *Environ Earth Sci*, 75(15):1120, August 2016.

[47] J Kolassa, R H Reichle, Q Liu, S H Alemohammad, P Gentine, K Aida, J Asanuma, S Bircher, T Caldwell, A Colliander, M Cosh, C Holifield Collins, T J Jackson, J Martínez-Fernández, H McNairn, A Pacheco, M Thibeault, and J P Walker. Estimating surface soil moisture from SMAP observations using a neural network technique. *Remote Sens Environ*, 204:43–59, January 2018.

[48] Prashant K. Srivastava, Dawei Han, Miguel Rico Ramirez, and Tanvir Islam. Machine learning techniques for downscaling SMOS satellite soil moisture using MODIS land surface temperature for hydrological application. *Water Resour Manage*, 27(8):3127–3144, June 2013.

[49] Paulin Coulibaly, Yonas B. Dibike, and François Anctil. Downscaling precipitation and temperature with temporal neural networks. *J. Hydrometeor*, 6(4):483–496, August 2005.

[50] Xiaogang He, Nathaniel W. Chaney, Marc Schleiss, and Justin Sheffield. Spatial downscaling of precipitation using adaptable random forests. *Water Resour Res*, 52(10):8217–8237, October 2016.

[51] Mitra Basu and Tin Kam Ho, editors. *Data Complexity in Pattern Recognition*. Springer Science & Business Media, illustrated edition, 2006.

[52] Kuai Fang, Chaopeng Shen, Daniel Kifer, and Xiao Yang. Prolongation of SMAP to spatiotemporally seamless coverage of continental u.s. using a deep learning neural network. *Geophys. Res. Lett.*, 44(21):11,030–11,039, November 2017.

[53] Sinno Jialin Pan and Qiang Yang. A survey on transfer learning. *IEEE Trans Knowl Data Eng*, 22(10):1345–1359, October 2010.

[54] Rajat Raina, Alexis Battle, Honglak Lee, Benjamin Packer, and Andrew Y. Ng. Self-taught learning: Transfer learning from unlabeled data. In Zoubin Ghahramani, editor, *Proceedings of the 24th international conference on Machine learning - ICML '07*, pages 759–766, New York, New York, USA, June 2007. ACM Press.

[55] Hoo-Chang Shin, Holger R Roth, Mingchen Gao, Le Lu, Ziyue Xu, Isabella Nogues, Jianhua Yao, Daniel Mollura, and Ronald M Summers. Deep convolutional neural networks for computer-aided detection: CNN architectures, dataset characteristics and transfer learning. *IEEE Trans Med Imaging*, 35(5):1285–1298, February 2016.

[56] Matthew E. Taylor and Peter Stone. Transfer learning for reinforcement learning domains: A survey. *Journal of Machine Learning Research*, 2009.

[57] Leo Breiman. Random forests. *Machine Learning*, 45(1):5–32, 2001.

[58] Seonyoung Park, Jungho Im, Sumin Park, and Jinyoung Rhee. AMSR2 soil moisture downscaling using multisensor products through machine learning approach. In *2015 IEEE International Geoscience and Remote Sensing Symposium (IGARSS)*, pages 1984–1987. IEEE, July 2015.

[59] Wei Zhao, Nilda Sánchez, Hui Lu, and Ainong Li. A spatial downscaling approach for the SMAP passive surface soil moisture product using random forest regression. *J Hydrol (Amst)*, 563:1009–1024, August 2018.

[60] Mary J. Brodzik, Brendan Billingsley, Terry Haran, Bruce Raup, and Matthew H. Savoie. EASE-grid 2.0: Incremental but significant improvements for earth-gridded data sets. *ISPRS Int J Geoinf*, 1(1):32–45, March 2012.

[61] D A Miller and R A White. A conterminous united states multi-layer soil characteristics data set for regional climate and hydrology modeling. *Earth Interact*, 2, 1998.

[62] NASA JPL. NASA shuttle radar topography mission global 3 arc second, 2013.

[63] S Kim. SMAP Ancillary Data Report on Landcover Classification, 2013.

[64] Myneni, R and Knyazikhin, Y and Park, T. MCD15A3H MODIS/Terra+Aqua Leaf Area Index/FPAR 4-day L4 Global 500m SIN Grid V006. Technical report, 2015.

[65] Wan, Z and Hook, S and Hulley, G. MOD11A1 MODIS/Terra Land Surface Temperature/Emissivity Daily L3 Global 1km SIN Grid V006. Technical report, 2015.

[66] Arthur Y. Hou, Ramesh K. Kakar, Steven Neeck, Ardeshir A. Azarbarzin, Christian D. Kummerow, Masahiro Kojima, Riko Oki, Kenji Nakamura, and Toshio Iguchi. The global precipitation measurement mission. *Bull. Amer. Meteor. Soc.*, 95(5):701–722, May 2014.

[67] Zhengming Wan and J. Dozier. A generalized split-window algorithm for retrieving land-surface temperature from space. *IEEE Trans. Geosci. Remote Sensing*, 34(4):892–905, July 1996.

[68] M. C. Peel, B. L. Finlayson, and T. A. McMahon. Updated world map of the köppen-geiger climate classification. *Hydrol. Earth Syst. Sci. Discuss.*, 4(2):439–473, March 2007.

[69] D Entekhabi, N Das, E Njoku, J Johnson, and J Shi. Algorithm theoretical basis document L2 & L3 radar/radiometer soil moisture (active/passive) data products, 2012.

[70] P E O'Neill, Steven Chan, Eni Njoku, Tom Jackson, and Rajat Bindlish. Algorithm theoretical basis document L2 & L3 soil moisture (passive) data products, 2015.

[71] Nandita Gaur and Binayak P. Mohanty. Land-surface controls on near-surface soil moisture dynamics: Traversing remote sensing footprints. *Water Resour Res*, 52(8):6365–6385, August 2016.

[72] Nandita Gaur and Binayak P. Mohanty. A nomograph to incorporate geo-physical heterogeneity in soil moisture downscaling. *Water Resour Res*, October 2018.

[73] A. Loew and W. Mauser. On the disaggregation of passive microwave soil moisture data usinga priori knowledge of temporally persistent soil moisture fields. *IEEE Trans. Geosci. Remote Sensing*, 46(3):819–834, March 2008.

[74] Tiejun Wang, Trenton E. Franz, Ruopu Li, Jinsheng You, Martha D. Shulski, and Chittaranjan Ray. Evaluating climate and soil effects on regional soil moisture spatial variability using EOFs. *Water Resour Res*, 53(5):4022–4035, May 2017.

[75] Tianqi Chen and Carlos Guestrin. XGBoost: A scalable tree boosting system. In *Proceedings of the 22nd ACM SIGKDD International Conference on Knowledge Discovery and Data Mining - KDD '16*, pages 785–794, New York, New York, USA, August 2016. ACM Press.

[76] R. H Reichle, G. D. Lannoy, R. D. Koster, Crow W. T., Kimball J. S., and Q. Liu. SMAP L4 global 3-hourly 9 km EASE-grid surface and root zone soil moisture geophysical data, version 4, 2018.